Claudia Verheyen
Faculty of Science
Department of Chemistry

PROMOTORS
Prof. Dr. Vasco Guerra
Prof. Dr. Annemie Bogaerts

MENTORS
Dr. Tiago Silva
Stijn Heijkers

Kinetic Modelling for a CO_2/H_2O-Plasma:

a Vibrational Kinetics Study

Masterproef ingediend tot het bekomen van de graad van Master in de Chemie

Academic Year 2017-2018
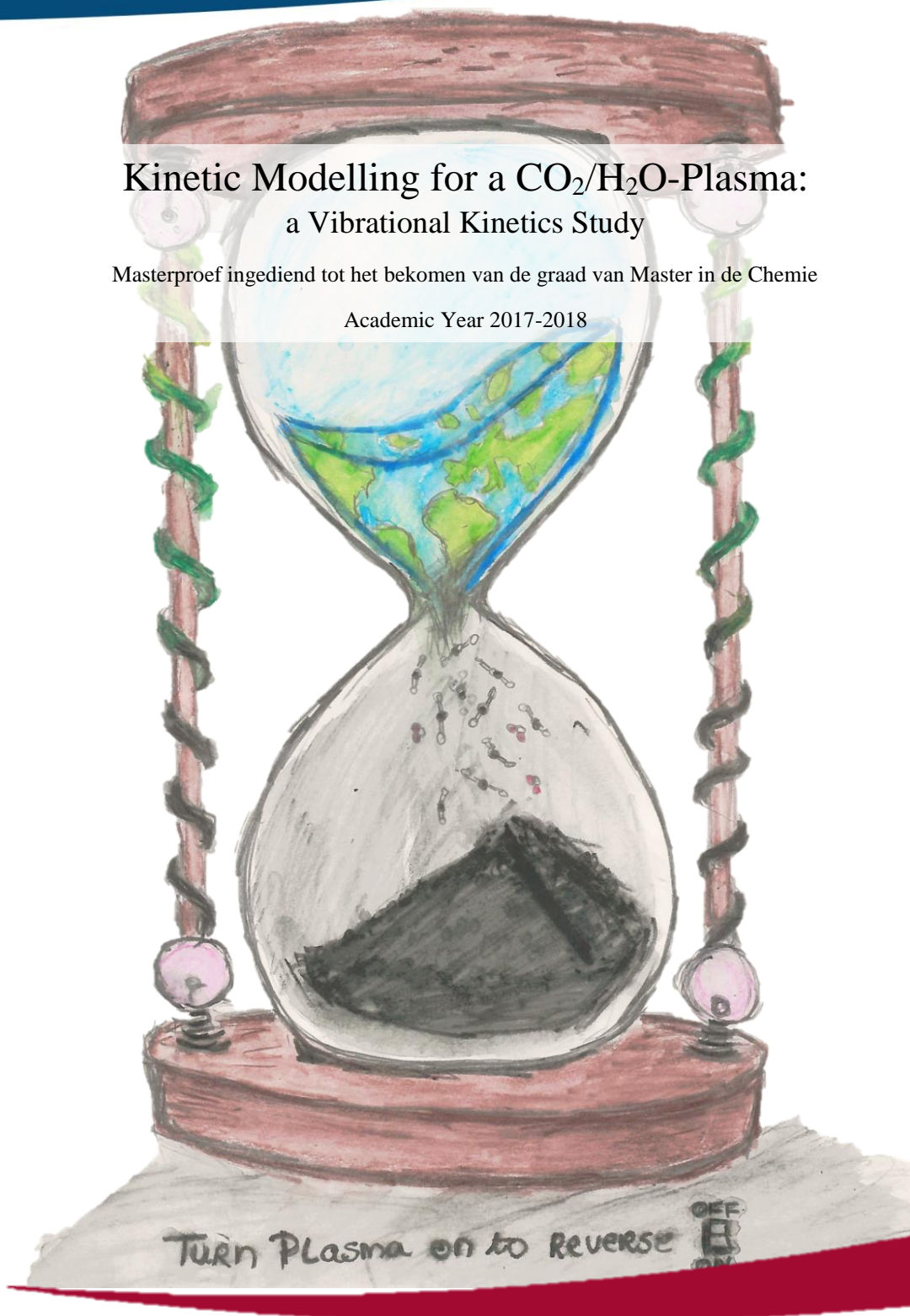
TÉCNICO LISBOA

ipfn
INSTITUTO DE PLASMAS
E FUSÃO NUCLEAR

PLASMANT
Plasma, Laser Ablation & Surface Modelling
Antwerp

Universiteit
Antwerpen

Look deep into nature, and then you will understand everything better.

Albert Einstein

Abstract

A kinetic modelling study was performed to obtain greater understanding of the vibrational kinetics of a CO_2/H_2O plasma. For this purpose, an electron impact cross section set for water was created using a swarm derived method. The study was performed using two kinetic models, developed by (i) Kozak and Bogaerts[1] and (ii) Silva et al.[2] Both were expanded by adding V-T-reactions with water.

The model of Kozak and Bogaerts[1] focusses more on the asymmetric vibrational levels of CO_2 up to the dissociation limit in a MW plasma. In this model (apart from V-T processes) we have included reactions involving electron impact. The results show a drop in the populations of the asymmetric vibrational levels of CO_2 upon addition of H_2O. However, the drop is less prominent than expected. Additionally, in the beginning of the plasma a small increase in the population of higher vibrational levels can be found. Possible explanations are (i) the higher electron temperature and (ii) the lower gas temperature upon addition of H_2O, which both contribute to a more favourable environment for vibrational excitation, and (iii) the influence of the electron impact reactions. Further studies and calculations are required to clarify this question.

The model of Silva et al[2] simulates the time-resolved evolution of the first 72 vibrationally excited CO_2 levels. This modelling tool has been already validated in a pure CO_2 glow discharge. In this master thesis, as a result of addition of H_2O, we observe an increase of the quenching of the CO_2 asymmetric levels. This is attributed to the addition of the V-T processes involving water molecules, which have rate coefficients much higher (> 2 orders of magnitude) than the rates involving collisions between CO_2 molecules. It is hard to compare the models due to (i) the use of different discharges, (ii) the calculations that are performed in the afterglow in the model of Silva et al. (iii) the difference in the vibrational levels included, (iv) the difference in the rate coefficients for CO_2 V-T and V-V energy transfers and (v) the lack of H_2O electron impact reactions. However, in general it can be stated that in both models a decrease in the vibrational densities occurs.

It can be concluded that H_2O addition to a CO_2 plasma shows a very interesting, but complex behaviour. Therefore, to better explain the results, a more extensive study of the different parameters is needed in the future.

Index

List of Abbreviations

CCS	Carbon Capture and Storage
CCU	Carbon Capture and Utilisation
CFC	Chlorofluorocarbon
CH_4	Methane
CO_2	Carbon Dioxide
CS	Cross Sections
DBD	Dielectric Barrier Discharge
DRM	Dry Reformation of Methane
EEDF	Electron Energy Distribution Function
GA	Gliding Arc
GAP	Gliding Arc Plasmatron
GHG	Greenhouse Gasses
H_2O	Water
H_2O_3	Carbonic Acid
IPCC	Intergovernmental Panel on Climate Change
LTE	Local Thermodynamic Equilibrium
MW	Microwave (Plasma)
N_2O	Nitrous Oxide
O_3	Ozone
SSH	Swartz, Slawsky, Herzfeld (Theory)
SST	Steady State Townsend

Chapter 1: Introduction

A. Global Warming

1. A threat to humanity

We all live on one Earth, and this earth is the only one we have. However, the last decades we lived like we have more of them. We are depleting the earth's fossil fuels faster than they are restored, tumbling us into a global crisis: climate change. According to the United Nations secretary general, António Guterres, climate change and global warming are the biggest threats to humanity.[3] They lead to drought, hunger, movements of people, and more extreme weather events. This again leads to wars and terror. As a side note can be made that global warming and climate change are not completely the same phenomenon, but are closely related to each other. Global warming focusses on the increase in the average temperature of the earth, while climate change is a partial consequence of this and is a broader term that includes also global warming, rising sea levels, melting ice caps, changes in climate patterns etc.

Climate change can be attributed to many different factors, of which the greenhouse gasses (GHG), and more precisely the increase of their amount in the atmosphere, have a major contribution. Greenhouse gasses can be defined as atmospheric gasses that absorb and emit radiation at specific wavelengths within the spectrum of terrestrial radiation (mostly in the thermal infrared range)[4], which causes them to basically trap heat within the earth's atmosphere and warm up the oceans (oceans take up 93.4% of the heat) and continental lands. GHG can be from a natural origin or can be human-made. The most known greenhouse gasses are carbon dioxide (CO_2), water vapour (H_2O), methane (CH_4), nitrous oxide (N_2O), and ozone (O_3). These gasses can be found naturally in limited amounts in the atmosphere (although also partially from an anthropogenic origin). Other greenhouse gasses that can be found, that are entirely of human origin, are halocarbons, of which the ozone-depleting chlorofluorocarbons (CFCs) are a part. If looked at the composition of the earth's atmosphere, one may notice that the greenhouse gasses are not very abundant and are just found in traces (less than 0.1% - except for water which concentration varies between 0-4%). As mentioned above, water (vapour) is also a greenhouse gas, but due to the fact that the atmosphere has its own way of getting rid of it, namely rain, the effect of it on global warming is limited (but can be seen in climate change).

An increase of the greenhouse gas concentrations is contributing to the greenhouse effect, which is a natural way to trap the radiation of the sun to make life possible. When solar radiation reaches the atmosphere, most of it will pass and reach the earth surface (figure 1). The rays that don't reach the surface will be reflected by aerosols and clouds. From the radiation that will reach earth's surface, some will be taken up by the oceans and grounds, but most will be reflected back as heat into space. However, some of the reflected radiation will be trapped by the greenhouse gasses. This is a natural process, the bigger problem here is that the amount of GHG has increased over the past few decades and therefore, the amount of heat trapped.
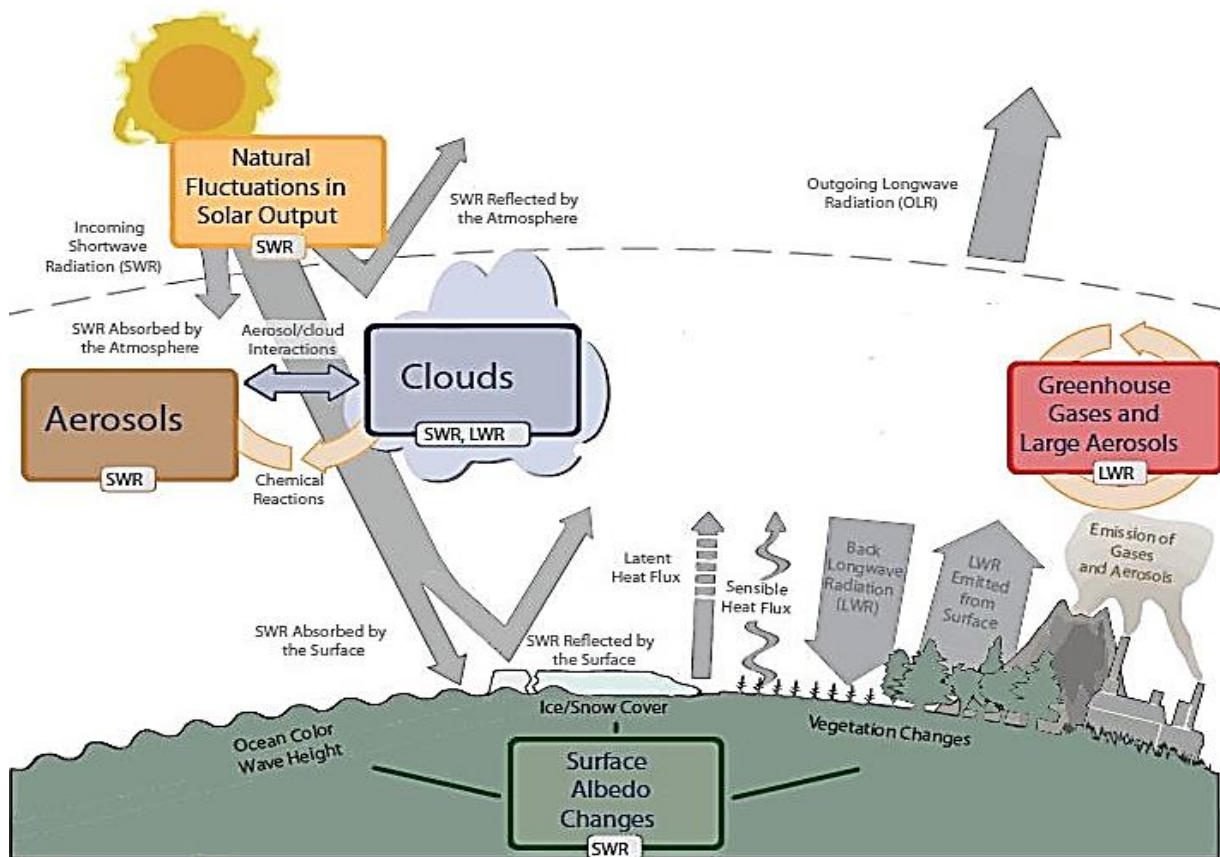
Figure 1: Schematic representation of the greenhouse effect. Solar radiation enters the atmosphere and can be either reflected by aerosols and clouds or reach the surface where it can be absorbed or reflected back..[4]

The most known and talked about greenhouse gas is CO_2. Although the CO_2-concentrations (around 0.038%) are not very high, its impact is many times greater. During last century, an increase of 40% can be seen compared to pre-industrial times (1750).[4] This contributes to an increase of the average earth's temperature with 0.85 °C from 1850 to 2012. Carbon dioxide is not only present in the atmosphere, but is part of a bigger system called the carbon cycle (figure 2), where it is exchanged between the earth's atmosphere, biosphere, pedosphere, geosphere, and hydrosphere.
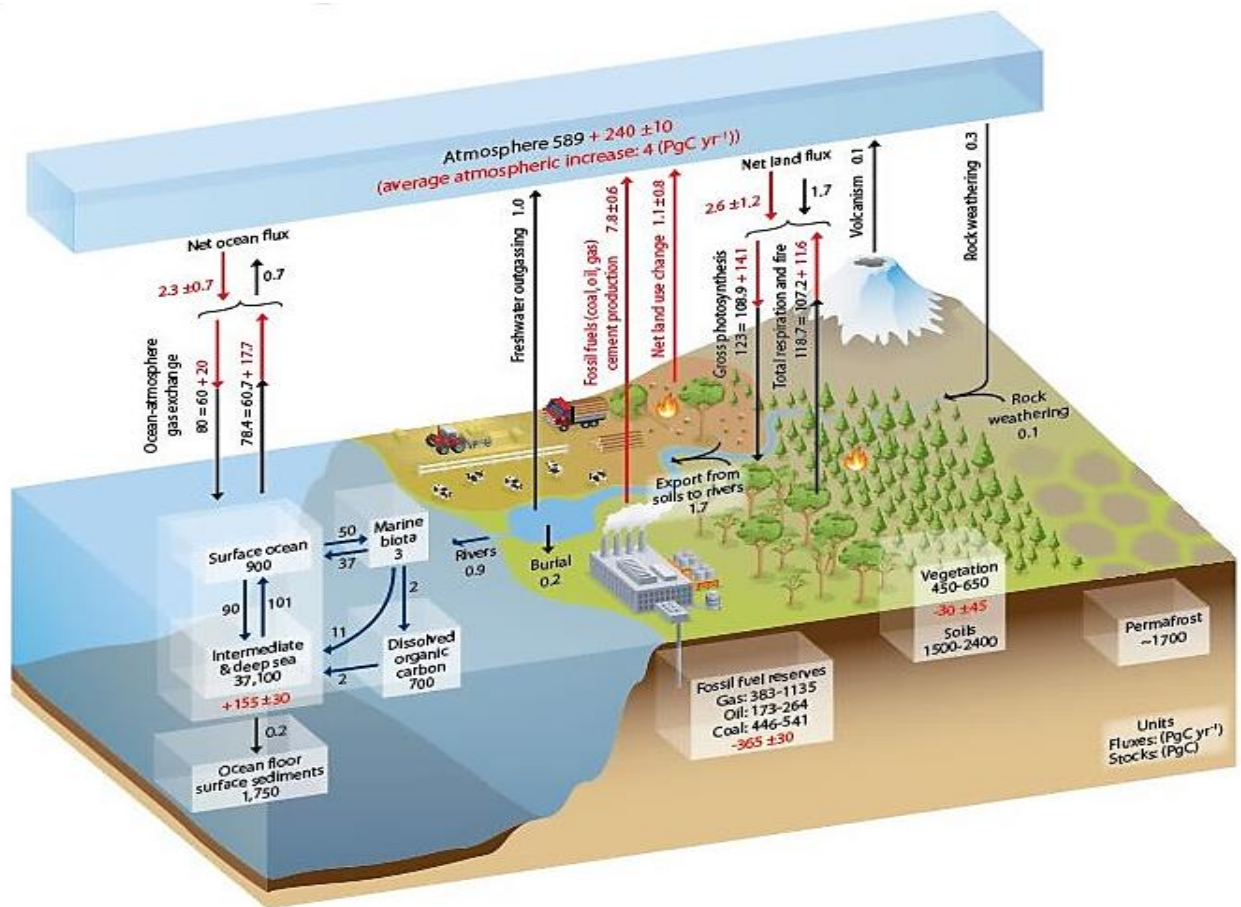
Figure 2 The Carbon Cycle. The different reservoirs and fluxes are shown, in which the ocean and the sedimentary rocks are the biggest.[4]

Carbon is an essential element needed for life on earth to exist, since it is the main component of biological molecules and compounds. Carbon from the atmosphere is taken in by respiration of plants and photosynthesis. After the plants die, it becomes part of the soil, or carbon is released again by burning into the atmosphere. Even though the total influx of carbon from anthropogenic sources is not large compared to the fluxes in the cycle, it is enough to tilt the balance. The biggest reservoirs of carbon are sedimentary rocks and oceans. The latter is very importantly interlinked with global warming since it takes up most of the heat from the radiation, but can also take up CO_2. The taken-up CO_2 is converted to carbonic acid (H_2CO_3), which later dissociates and releases H^+. This is a normal process, but due to the extra CO_2 in the atmosphere, more CO_2 enters the oceans (it has taken up 30% of the extra emissions[4]) and therefore more H^+ is released, causing the acidification of the oceans. Another mechanism is related with the disruption of shell formations of some marine animals. H^+ will bind to CO_3^{2-}, which is an important compound needed to make the shells ($CaCO_3$) and so interfering with the

3

shell formation for some marine animals. Moreover, the extra acidic water will start to dissolve the shells ($CaCO_3$) and break them down. The shells would normally also sink down and become part of the surface again once the animal died, and by doing so immobilizing the carbon. This all causes that even though there is more CO_2, less of the carbon can be immobilized by marine animals. The important lesson here is that environment cannot cope with the increased influx of carbon itself. The increased temperature triggers mechanisms that just trigger more GHG release (another example is the melting permafrost that causes the release of carbon in forms like methane that was stored within).

2. Short History of Climate Change[5]

It took a while for the politics and public to wake up. The earth is known to have gone through climate changes since the beginning of its formation. The very known ice ages serve as a good example, but even closer to our times there even was a medieval warm period. So, when the first warnings were made of a possible climate change, not many where alerted. The idea that mankind could induce a change in climate was a step too far for many. This did not stop scientists anyhow of investigating the earth's climate and the influence of mankind on it. In 1896 Svante Arrhenius published his article *On the Influence of Carbonic Acid in the Air upon the Temperature of the Ground,*[6] and is one of the first to acknowledge and quantify that the amount of CO_2 in the air and the temperature are connected, a new idea at that time.

In the 20th century, changes started to be noticed, not linked yet to the introduction of extra carbon to the atmosphere by man. Until 1937, when Callendar discovered what we now call global warming, an increase in earth temperature.[7] He linked the increase of temperature to the fact that most of the CO_2-emissions stayed in the earth atmosphere and predicted that the increase would continue with $0,003 – 0,005°C$ per year.[7] At that time the idea of having an increased temperature was seen as beneficial, since it would stop a next ice age. This discovery sparked more interest in the changes that were ongoing in the earth atmosphere. This led to exact measurements of CO_2 concentrations in the atmosphere. In 1960 Charles D. Keeling published that a persistent rise in CO_2-levels could be found, independent from the seasonal variations.[8] The curve showing that increase is now called the Keeling curve (figure 3). Because of the coal burned, also lots of small particles entered the atmosphere, creating a cooling effect. This warming on one side and cooling at another sparked a lot of confusion between scientists and the public. The different factors included made it very hard to create a model that would correctly predict the course of the warming.
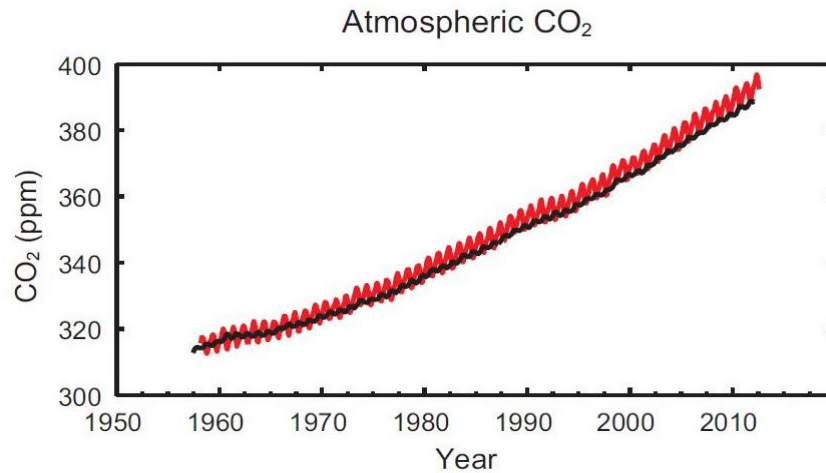
Figure 3: Keeling Curve – The steady increase in CO_2-concentration over the years with seasonal fluctuations.[4]

In 1988 the United Nations set up the Intergovernmental Panel on Climate Change (IPCC) to provide the world with an objective and scientific based view on climate change and its consequences. By that time, it was also already accepted that global warming was most likely manmade - it took some more years before it turned into very likely. Climate change quickly became a global issue that could only be resolved by all countries working together. In 1997, the first big international breakthrough for cutting down GHG levels was made: the Kyoto Protocol. Industrial countries (38 in total) agreed on cutting down the GHG by 5.2% below 1990 levels between 2008 and 2012, but already in 2001 the USA, followed by Canada, Japan and Russia withdrew. Developing countries like India and China refused to agree to any reductions, since the cause of the problem lays within the industrial world. It took many more conferences (Bali, Copenhagen, Cancun, Durban, Doha) before a comprehensive climate agreement was established in 2015 in Paris, known as the Paris Agreement. The Paris Agreement strives to keep the increase in temperature under 2°C above pre-industrial levels, but the goal is to keep the increase under 1.5°C. It also focusses on increasing the ability to adapt and fight climate change and funding for developing countries. All countries will have to make an effort and submit their nationally determined contribution to combat climate change.

Worth mentioning is also the influence the public's opinion plays into this and therefore the documentary *An Inconvenient Truth* (2006). Al Gore's documentary brought climate change closer to the people and was a wake-up call for the public. It made climate change not a case only scientists work on, it raised public awareness, and it showed we all have an influence on the climate. There is no more doubt that climate change is happening, even the biggest deniers cannot look past all the scientific evidence, ranging from biological indicators to isotope

fractionation. As well as the the disempowerment of the argument that the cause is natural, caused by natural cycles, like reoccurring glacial stages and Milankovitch cycles. Although a lot is already known about climate change and the forces that drive it, still a lot of uncertainties exist. New drivers but also inhibitors are discovered regularly, and this contributes to the uncertainties in the models to predict the development of climate change in the future. Another uncertainty are the measures (by governments as well as by the public) that will be taken to tackle climate change and if they will be enough. However, it can be stated with certainty that if nothing is done, the temperature will rise far over the maximal 2°C limit (figure 4).
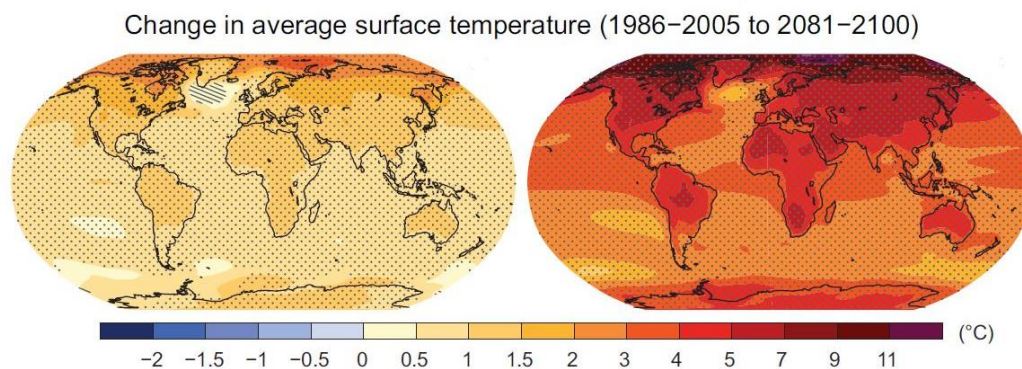
Figure 4: Two possible scenarios for the increase in average surface temperature – Left: assuming GHG emissions will peak between 2010-2020. Right: assuming the emissions will continue to rise throughout the 21st century. [4]

3. Solutions

There are two ways to follow while fighting climate change: mitigation and adaptation. Mitigation is a way to reduce the amount of GHG that will enter the earth's atmosphere, by intervening at the sources or creating more sinks for the GHG, while adaptation, as the word says, is trying to adapt to the change that already exists. The use of renewable energy can be seen as a way of mitigation. The sources are divergent like solar, wind, tidal or hydro energy. The biggest advantage they have is that they are naturally unlimited. The biggest drawback is that the supply is not constant over a big period of time (solar energy can be only harvested during the day) leading to storage and supply problems. Nevertheless, the European Union set a target for 2020 that 20% of the final energy consumption should come from renewable energy.[9] This implementation for energy supply can be the first step to create a low carbon economy. Another example of mitigation can be ocean nourishment, where algae bloom is triggered. Algae capture CO_2 and when they die, part of it sinks with the dead algae to the bottom of the sea. Another way to go is geo-engineering, like solar radiation management, where scientists try to reduce the amount of sun radiation that reaches the earth (or stays in the earth's atmosphere) by putting metal reflectors on earth, and so increasing it is albedo

(increasing the amount of radiation that is reflected). Other techniques include increasing aerosols in the air, and so decreasing the amount of radiation that reaches earth's surface. The examples mentioned above are just a few of a whole range of ways and techniques scientists have developed to battle climate change. Closely related to mitigation is carbon dioxide removal where CO_2 is directly captured from the atmosphere by increasing sinks or removing it by chemical engineering. The carbon captured (from the flue gasses or directly from the atmosphere) can be stored underground (carbon capture and storage, CCS), as is now a quite common technique, although the risks are not yet completely known, but can include leakage,[10] and consequently there is always a possibility for the CO_2 to be released again. Another way to go is using the captured CO_2 to recycle (carbon capture and utilisation, CCU) it into industrially interesting products like syngas (gas mixture of mainly CO and H_2) or other more complex substances, like biodiesel or methanol that can store energy. This would be a solution for the energy storage problem that occurs while using renewable energy or surplus energy of the industry. Among different ways that can be used to recycle CO_2 (photo-chemical driven conversion, thermochemical conversion, solid oxygen electrolyser cells, etc.), the splitting of the CO_2-molecule using plasma technology (also known as plasmolysis) is extremely interesting.[11,12]

As discussed in Goede et al.[11] and Snoeckx and Bogaerts,[12] plasma has many technological advantages: (i) it does not require the use of scarce materials, (ii) it allows fast switching and the connection with intermittently renewable energy, (iii) it can work at room temperature and (iv) it is scalable to large units to the size of the energy market. For these reasons, CO_2 conversion by plasma has been extensively studied in the past years through both modelling studies[13–15] and experimental works.[16,17] In fact, this master thesis will be part of this bigger plasma research that is ongoing to understand the mechanisms of CO_2 conversion and gain more insight into it. More specifically, in this work, we study the influence of mixing H_2O with CO_2 for the purpose of forming fuels that can be used for energy storage applications[11]. Even though this is only a small part of a bigger project, that is only one of the many ways to fight climate change, it is important to remember that many small things make one big, and every effort into fighting one of the biggest threats to humanity counts. In the next section, we give a general overview on plasmas, while subsequently, the state of the art related to the use of plasma for CO_2 conversion will be presented.

B. Plasma[18]

Everyone knows plasma, even though sometimes they don't realise it. Plasmas are everywhere, we are surrounded by them and even more than 99% of the visible universe consists of plasma. Those daily life plasmas can range from watching Netflix on a plasma screen to just enjoying the sun on a warm summer day, since the sun and stars are plasmas too. Even though plasmas are so common, the term plasma is more connected by the public to blood plasma than by this curious phenomenon. It is not surprising this confusion exists, since the word plasma is derived from blood plasma. In 1928 Irving Langmuir introduced the term plasma, because of the resemblance of it to blood plasma by the multicomponent aspect. Plasmas are ionized gasses, containing all different kinds of species, like charged particles (electrons, positive and negative ions), neutral molecules, excited species, radicals and UV photons. Due to this composition, plasma has distinct properties and qualifies as the fourth state of matter, apart from solid, liquid and gas. Even though plasmas are electrically neutral, they still are electrically conductive, as a result of the free charges (electrons and ions) they contain. Not all the particles have to be ionised, most of the time plasmas on earth have an ionisation degree of 10^{-7} to 10^{-4}, but completely ionised plasmas also exist. Those completely ionised plasmas are often found in thermonuclear applications, like plasma fusion tokamaks. On the other hand, plasmas with a low ionization degree are called weakly ionized plasmas.

Electrons play a very important role in the plasma, since they are charged and have one of the lowest masses. They will take up the applied electrical energy at first, and later distribute it due to collision to more heavy partners. The electron densities in plasmas vary between 10^6 and 10^{18} cm^{-3} and their temperatures cover a range from 1 eV to 20 eV (1 eV is around 11 600 K). Electrons will acquire energy during their mean free path. They also will lose energy due to collisions, but owing to their low mass that amount will be limited in elastic collisions. In inelastic collisions the energy loss is greater, but their cross sections are typically smaller, so the effect is also limited. Therefore, the electrons will have their own electron temperature, which in the case of non-thermal plasma (see further) is some magnitudes higher than the gas temperature.

The temperature of the plasma will be determined by the particles and the relevant degrees of freedom. Those particles can be in thermal equilibrium or not. This equilibrium can be a result of Joule heating. When an electric field is applied, the electrons will be accelerated. Owing to

the fact that electrons are lighter than the other (heavy) particles like molecules, the electrons will receive more kinetic energy. The heavy particles will acquire energy by elastic collisions with the highly energetic electrons. As a consequence of the mass differences, the energy transfer will not be very efficient, creating therefore a difference in temperature between the species. However, if the residence time or the pressure is high enough; more collisions will occur and so creating a thermal equilibrium. A plasma where this quasi-thermal equilibrium or equilibrium occurs, is called thermal or local thermodynamic equilibrium plasma (LTE). In LTE plasmas therefore, the temperature is equal for all the different species.

If the equilibrium is not obtained, and plasmas can exist far from equilibrium, the plasma is called non-thermal. As mentioned before, the electrons in the plasma will have a higher temperature than any other particle. Electrons in a non-thermal plasma have an average energy of around 1-10 eV, while the gas temperature can be just around room temperature. After the electron temperature, the temperature of vibrational excitations of molecules is the second highest. The heavy neutrals (the gas temperature or translational degrees of freedom), ions and rotational degrees of freedom of the molecules have the lowest temperature. A non-equilibrium can be generated using low pressures (but even up to atmospheric pressure), lower power levels or pulsed systems.

There exist many ways to create plasmas. Typical plasma reactors used in research on CO_2 splitting are dielectric barrier discharges (DBD), gliding arc (GA) plasmas, microwave (MW) and glow discharges. As the name already predicts, in DBD a dielectric barrier like glass, quartz or ceramics is used. This barrier counteracts the formation of sparks, and therefore a DBD is also called a silent discharge. The build-up of a DBD can be planar or cylindrical and it consists of electrodes (high voltage and ground electrode) with the dielectric barrier, that can exist out of more layers, in between (figure 5 – left). It requires an AC-voltage to operate. The characteristics of this discharge are that it is in a strong non-equilibrium at atmospheric pressure at reasonably high-power levels. The DBD can be modified by adding dielectric pellets, to form a packed bed DBD. A GA plasma is an auto-oscillating periodic discharge. In a classical GA, an arc plasma is formed in the narrowest gap from the gas flow between two diverging flat electrodes with a potential difference (figure 5 – right). It is a continuous cycle where the small arc becomes bigger due to being dragged upwards by the gas flow up to increasing interelectrode distance, while a new small arc is formed when it fades away. A GA plasma can be thermal or non-thermal depending on the power and flow rate. Apart from the 2D version,

that shows disadvantages for industrial use, other 3D cylindrical set-ups exist that make use of a vortex gas flow. Another set-up that can be used for CO_2 splitting is a glow discharge (figure 6 – left). It can be defined as a luminous DC discharge that is self-sustained and continuous with a cold cathode which emits electrons as a result of secondary emission, mostly induced by positive ions.[18] It consists of a cathode layer, with a positive space charge and strong electric field, and an anode layer characterized by a negative space charge. Finally, electrodes are not always needed to create plasmas, an alternative way is to use electromagnetic radiation in the frequency range of 300 MHz to 10 GHz, the so-called microwaves. The microwaves will penetrate the plasma and make the electrons gain energy. This creates a microwave plasma (figure 6 – right). This is only possible when the electron density is lower than the critical electron density (around 7.6×10^{16} m^{-3}). Microwave plasmas can work with different pressures ranging from 1 Pa (for electron cyclotron plasmas) to atmospheric pressure.
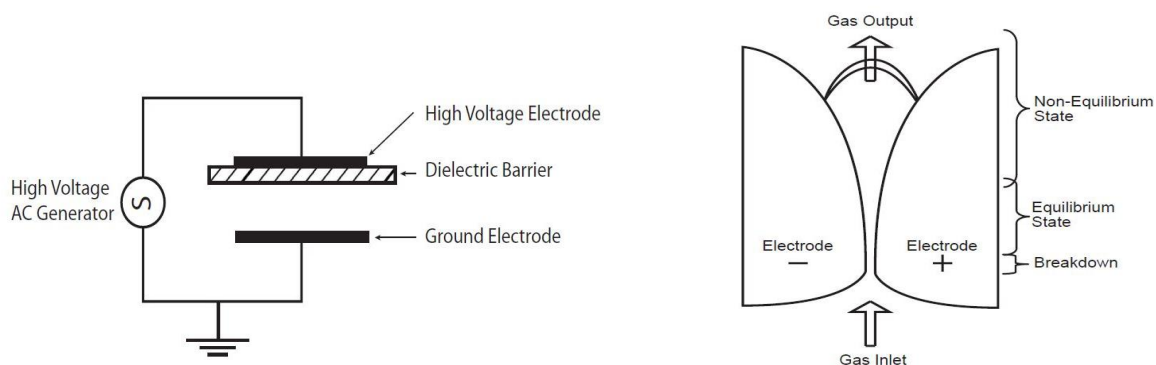
Figure 5: Schematic representation of a DBD reactor (left) and of a classical GA (right).[18]
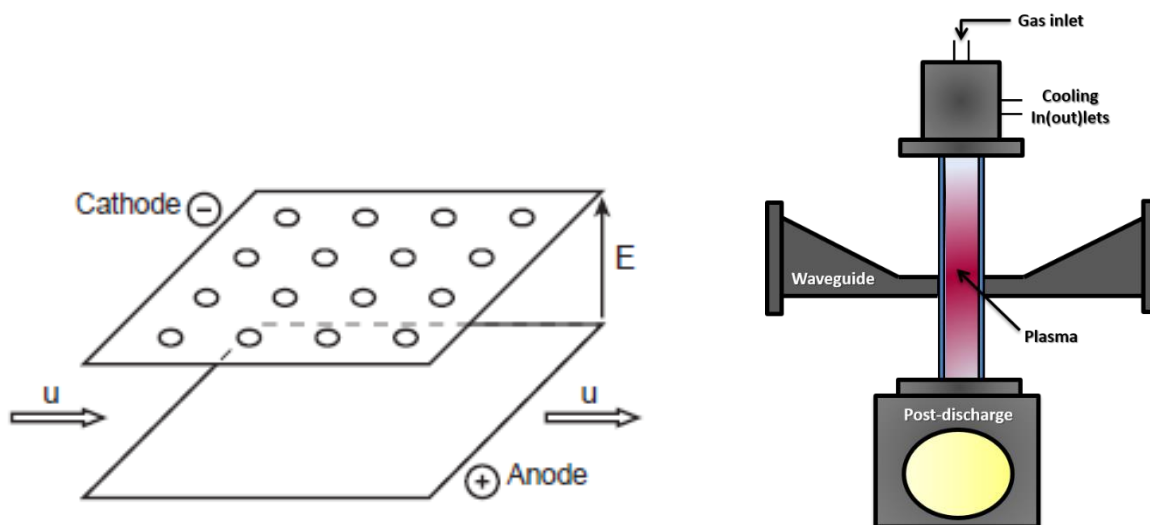
Figure 6: Schematic overview of a glow discharge set-up[18] (left) and a MW-plasma set-up[14](right)

C. State of the Art of CO₂ Conversion Research

The idea of converting CO_2 into value-added products with plasma originates from 1970. During this period, Fridman et al.[18,19] conducted major research efforts in order to gain a deeper understanding of different plasma operation conditions, that enhance molecular decomposition. Their motivation was fourfold. First of all, studying CO_2 conversion can be beneficial to gain insight in the dissociation in CO_2 lasers. On the other hand, there is the interest in gaining more fundamental insight in the stimulation of vibrational excitation with high energy efficiency. A third motivation is that CO_2 dissociation can become a model for more complicated processes like the reduction of metals from their oxides and halogenides. At last, there is the economic aspect, where CO_2 can be used to create value-added products like fuels. Plasmas are a very handy tool for this purpose, since by controlling different parameters, like the electron density and temperature and the gas temperature, specific reaction channels can be enhanced or suppressed, and therefore one can control the way the dissociation reaction occurs. During the seventies and the eighties of previous century, research was conducted to optimize the energy efficiency of the conversions.

For thermal plasmas, the theoretical highest efficiency that could be achieved, back in the eighties, varies between 43% and 48% and the experimental around 15%. These values are not high enough, and so based on these results the non-thermal plasma approach was chosen. The reason behind this low numbers is that by using a thermal plasma, the input energy will be (roughly) equally distributed among all reaction channels. This includes reaction channels that are not useful for dissociation. On the other hand, by using non-thermal plasmas, selectivity can be created and it can be tuned to enhance certain channels by changing the operation conditions, and so where the energy goes to. In these plasmas, still different options exist. For low-pressure discharges (like a glow discharge), the efficiency was still not optimal, owing to mostly channelling the electronic excitation. With the use of more moderate pressures (50 - 300 Torr), higher values of energy efficiency can be achieved. By playing with the reactors, efficiencies between 60% for pulsed microwave discharges and radiofrequency discharges, to 80-90% for microwave plasmas could be achieved, for specific conditions, e.g., by using supersonic gas flow. In general, it can be said that among various plasmas (thermal and non-thermal) used for CO_2 dissociation research, microwave plasmas possess the highest efficiencies associated with molecular decomposition, achieving 80-90% according to Asisov et al.[20]. These high efficiencies are the result of a combination of relatively high electron density and low reduced

electric field, which favours the selective excitation of the asymmetric vibrational levels of CO_2.[18]

Apart from plasma, it is worth mentioning that other alternative routes can be used to convert CO_2. First of all, CO_2 can be converted thermally, but since CO_2 is a stable molecule, the energy input needed is 283 kJ/mol and so relatively high. Therefore, removal of the products (since the equilibrium is in favour of CO_2-formation) and high temperatures are needed. A way to optimize this reaction is the use of a co-reactant like CH_4 or H_2. Other approaches that can be used are electrochemical conversion (using a potential difference between two electrodes) or the use of solar energy for thermochemical and photochemical conversion. Both use solar energy as input, but the difference lays in how that energy will be used. For thermochemical conversion, the energy will be absorbed as thermal energy and for the photochemical quantum conversion, the energy of a photon is required with the use of absorbers like semiconductors. Another way to go is using biochemical conversion to produce biofuels. A drawback here is the competitiveness with the food supply, since biofuels can use up land that could be used for food production, so an alternative is the use of microalgae, but until now the costs of cultivation are still high. To end, also catalysts can be used to convert CO_2 (sometimes in combination with plasmas, in so-called plasma-catalysis). Overall, all the methods have advantages and disadvantages, just like plasma, but due to its unique features and since no scarce materials are needed, plasma is a very interesting method to focus on.[12]

Nowadays, and given the necessity to respond to the already mentioned global warming issues, the research related with CO_2 conversion by plasma has been considered an important and hot topic among the plasma science community.[21] To this purpose, many types of reactors, such as DBDs, gliding arc (GA) and microwave (MW) plasmas have been lately utilized for the study of CO_2 decomposition, with various energy efficiencies reported. For instance, Spencer et at.[22] have used MW discharges at atmospheric pressures to convert CO_2 with efficiencies of about 20%. Nunnally et al.[23] have used GA plasmas (also at atmospheric pressure) to convert CO_2 with an efficiency of about 40%. On the other hand, DBDs usually provide lower energy efficiencies (typically 5-10%, see e.g. Aerts et al.[24]).

In spite of the past and recent efforts, the application of these discharges is not yet well understood and not yet well optimized for the massive CO_2 decomposition needs. For this reason, in order to improve our understanding of CO_2 conversion, there is a constant need to

develop and improve models that simulate and predict the overall behaviour of CO_2 discharges. In this context, from a theoretical point of view, CO_2 conversion has been studied extensively by different research groups over the world. For instance, at the group PLASMANT (University of Antwerp) an 0D kinetic model was developed by Kozak and Bogaerts.[1] This model reveals the importance of the vibrational excitations and gains a further understanding of it, as well as the plasma physics and chemistry. It is also a tool to optimize the conversion and energy efficiency. In addition, the N-PRiME (University of Lisbon) have recently developed a state-to-state model to describe the evolution of the lower lying CO_2 vibrational levels in a glow discharge.[2]

Another important factor often studied is the effect of discharge mixture. The use of mixtures can have different advantages. A very important factor here is the price associated with the CO_2 conversion. Since the input is CO_2-gas, the sources will differ. Note that CO_2 can be captured from fumes and exhausts or can be captured from the atmosphere, in either one CO_2 will not come in pure form, so it will need to be separated out of it, which will be an additional cost. So, using mixtures might reduce the cost. Another advantage, depending on the gas, can be that the added gas might introduce benefits for conversion and efficiency and even create different new products. Adding a gas can also have a disadvantage that it can depopulate the excited vibrational levels, an important mechanism for dissociation. Therefore, adding new gasses to the mixtures has an influence on how electron energy is distributed among the different dissociation channels. Until now, most research has been done with CO_2-mixtures with methane (dry reformation), H_2 (hydrogenation), N_2 and H_2O. Below we will discuss each of these cases.

Dry reformation of methane (DRM) has been studied most extensively.[12] Due the extra products, it is harder to understand and the CH_4/CO_2 ratio plays a big role. Depending on the mechanism, different products can be obtained. Using only one step, oxygenated hydrocarbon products like methanol, formaldehyde, dimethyl ether and formic acid can be formed, while using two steps, syngas produced in the plasma can be transformed post-plasma in Fisher-Tropsch liquids and methanol.[12] Due to the diversity of products, it is harder to calculate the energy efficiency, and therefore, it will be reported in energy cost per converted molecule.[12] For DBD, the highest conversion reported in a non-packed DBD is 66%,[25] and the lowest energy cost is 16.4 eV.[26] For a packed-bed DBD the best over results found in literature are a total conversion of 45-60% with an energy cost of 13-16 eV.[27] Thus, the downside of DBDs is this high energy cost.[12,25,27] For MW discharges, high conversions of 79% with an energy cost

of 6.5 eV have been reported by Cho et al,[28] but besides this, they have not been studied extensively in literature yet. They show a selectivity for CO and H_2.[12] Using GA, mostly syngas and C_2 hydrocarbons and solid carbon are formed.[12] The best overall results show a conversion of 39% with an energy cost of 1 eV,[29] but these conversion values can be increased with ~20% upon use of a catalyst.[12,30] Note that the energy cost is significantly lower than the one obtained by DBD. Compared to DRM, the use of H_2 is only studied in limited amounts,[12] since H_2 is a quite expensive gas. The few research papers for this mixture show conversions around 2-3 times lower than the ones for pure CO_2 or DRM.[12,31,32] The main products formed are CO and H_2O.[12]

There can be many reasons for why researchers choose to add N_2 to a CO_2 mixture.[12] One of them is to stimulate ignition or to mimic real effluent gases, as N_2 is often an important component in real gas mixtures. This can be done since N_2 is an inert gas. N_2 can also have beneficial effects on the conversion of CO_2. In a DBD reactor, a fraction up to 50% N_2 does not influence the effective conversion rates or the energy efficiency, even though the concentration of CO_2 is lower. This is because the CO_2 molecules dissociate when they collide with a N_2 metastable molecule.[15] In MW plasmas,[14] N_2 also shows beneficial effects and increases the absolute conversion of CO_2 by contributing to the population of the lower vibrational levels. This population of the lower levels occurs as a result of the small energy difference between the first vibrational levels of N_2 and CO_2, making a fast resonance transfer of vibrational energy possible.[33] As a result, N_2 helps with pumping the asymmetric vibrational levels that lead to dissociation.[14] An important side effect of the use of N_2 is the creation of NO_x compounds as unwanted by-products that lead to severe air-pollution, which is a big downside.

Since H_2 is a quite expensive hydrogen source, the use of H_2O also might be quite interesting. It is typically also present in industrial fumes. The use of H_2O has been mostly studied in DBD. The results showed that the use of water mostly leads to lower conversions of CO_2.[34,35] In the case of MW plasmas, this can be up to around 12-25%.[36] This is due to the fact that H_2O probably quenches the vibrational levels of CO_2. The main products are H_2, CO and H_2O_2, the latter can be used as a disinfectant in medical applications.[34] It was not possible to make oxygenated hydrocarbons yet. If CO_2 and H_2O are converted simultaneously, the reaction is referred to as artificial photosynthesis. Even though some research was done into the usage of H_2O, it is still only very limited compared to pure CO_2 conversion or DRM. Still, many questions arise and further research into the reactions of this mixture and how they interact may

give us interesting insights into this reaction. It might be particularly interesting to understand the interaction of H_2O with the vibrational levels of CO_2. This master thesis research will, therefore, follow that path.

D. Aim of This Master Thesis

As will be explained in more detail in Chapter 2.A, the vibrational excitation of CO_2 plays an important role in the conversion of CO_2. For this reason, it is an interesting starting point for this research. A handy tool for this analysis is based on computational methods since they allow to study the influence of various plasma parameters. For this thesis, a new reaction set will be created that is focussed on the reactions between H_2O and CO_2, where H_2O plays the role of a collision partner. The focus will be on the influence of H_2O on the vibrational levels. A step-by-step approach will be used by including as first the V-T-reactions. Next, the influence on the vibrational densities will be verified. By doing this, the influence of the V-T-reactions can be tested before moving on to a more extended model. It was reported before that water lowers the conversion of CO_2, therefore we expect water to quench the vibrational levels.

The first step in this research is finding good cross sections for the electron impact reactions of H_2O. Subsequently, we will look into the addition of a H_2O/CO_2-kinetic scheme that can be included on the models developed by Kozak and Bogaerts[1] and Silva et al.[2]

The thesis is built up as follows. In chapter 2 (Theory and methods), more information will be provided on the molecules and background information about the calculation methods used. In chapter 3 (Results and discussion), the modus-operandi will be discussed for obtaining an H_2O-cross section set and the results of the modelling will be discussed. In Chapter 4, the conclusion and future prospects will be provided.

Chapter 2: Theory and Methods

A. Background

Plasma research through modelling has many important advantages. First of all, from an economic point of view, the use of plasma simulations can save a lot of money and time. For instance, the set-up of a plasma reactor can be optimized as a result of using optimal conditions (gas pressure, reactor dimensions, etc.) provided by modelling studies. On the other hand, depending on the dimensions of the plasma reactor or operation conditions, the study of the plasma system through experimental diagnostics (Langmuir probes, optical emission spectroscopy, etc.) might be limited or in some cases even impossible. Under such scenario, the use of simulations can overcome these difficulties. It is also worth mentioning that experimental diagnostics often provide average values of physical quantities (e.g. electron density, gas temperature, etc.). Consequently, a more complex and detailed description of the plasma system would require modelling research. In the end, it is important to realize that it is not possible to create models that describe all the physical and chemical laws. Approximations must be made to keep the work running. Even though simulations are not perfect (just like experiments), they can describe the reality in a good manner and provide insights that would be otherwise unreachable.[37]

1. The CO_2-molecule

A. General
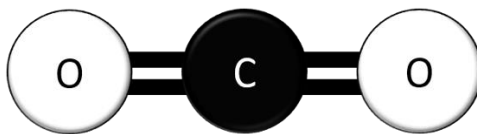
Figure 7: Schematic representation of a CO_2-molecule

The carbon dioxide (CO_2) molecule is well-known by the public and extensively studied by the scientific community, as a result of its relation to climate change. This section will provide some background information required for the understanding of this molecule.

CO_2 is composed of three atoms (see figure 7): one carbon atom in the middle connected by double bonds to two oxygen atoms, giving it a total mass of 44.0095 g/mol. If measured from ground state, the dissociation energy (breaking a C=O-double bond) is 5.451 eV and the energy needed for ionization is 13.777 eV.[38] With its three atoms and because of its linearity, CO_2 is a

symmetric molecule, with the symmetry along the nuclei and a plane of symmetry perpendicular to its axis. Even though the C=O bond is polar, as a result of the symmetry, CO_2 will have no permanent dipole. CO_2 is due to its linearity also a linear rotor. The rotation will occur only about the axis perpendicular to the line of atoms. A rotation of 180° will also result in an indistinguishable state of the molecule. Since it is a nonpolar polyatomic molecule, it will be rotationally inactive.[39]

An important aspect of this molecule for current research is related to its vibrational modes. It is important to note that CO_2 is a linear triatomic molecule with 4 normal modes of vibration (according to the formula $3N - 5$ with $N = 3$). These modes of vibration include one mode of symmetric stretch, two degenerate (levels with the same energy, due to the linearity) bending modes and one asymmetric stretch mode (figure 8). Each of the main modes (symmetric stretch, bending, asymmetric stretch) will be specified by a vibrational quantum number v, (v_1, v_2, v_3) respectively.[39] The double degeneracy will be denoted by an extra vibrational angular momentum quantum number, since the degeneracy causes an angular momentum around the molecular axis. Therefore, the quantum number will be associated with the resulting angular momentum and can take up value:[38]

$$l_2 = v_2, v_2 - 2, \dots \text{until 1 or 0 depending on if } v_2 \text{ is odd or even} \qquad (1)$$

The infrared absorption spectrum shows bands at 667.3 cm^{-1} and 2349.3 cm^{-1} that correspond to v_2 and v_3 respectively. The v_1 mode is not infrared active, because it does not change the dipole moment. However, v_1 changes the size of the molecule and therefore the polarizability and is thus Raman active. The Raman spectrum shows a band at 1340 cm^{-1}, that can be resolved into two peaks at 1285.5 cm^{-1} and 1388.3 cm^{-1}. It is important to mention that due to the exclusion rule (if the molecule has a centre of symmetry, no modes can be both infrared and Raman active), only one v_1 peak should be expected. One can notice that the average of the peaks is remarkably very close to the value of double v_2, because of which Fermi resonance (shift in the absorption bands due to quantum mechanical mixing) occurs.[38] As a consequence, the levels $(v_1, v_2^{l_2}, v_3)$ and $((v_1 - 1), (v_2 + 2)^{l_2}, v_3)$ will be Fermi coupled. Note that only levels with the same l_2 can be Fermi coupled.[40] The description related with the calculation of the energy of these CO_2 vibrational levels is given below.
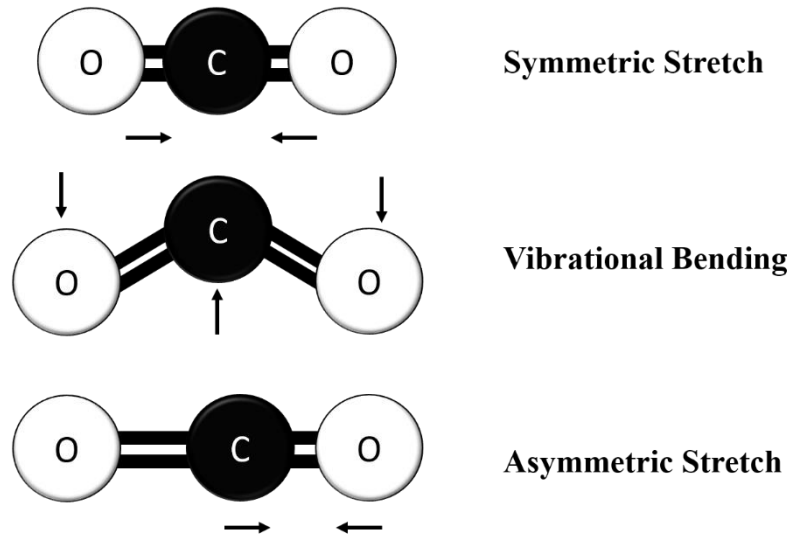
Figure 8: Schematic representation of motion of the vibrational levels of CO_2.

B. Calculation of the Energy Levels

The energy levels are calculated in this work using the anharmonic oscillator approximation.[1] As a consequence, the energy levels are not equally spaced at higher vibrational excitations. The formula to calculate the energy levels is as follow:[41]

$$\frac{E_{CO_2}}{hc} = \sum_i \omega_i \left(v_i + \frac{d_i}{2} \right) + \sum_{j \geq i} x_{ij} \left(v_i + \frac{d_i}{2} \right) \left(v_j + \frac{d_j}{2} \right) + x_{l_2 l_2} l_2^2 \tag{2}$$

The spectroscopic constants $(\omega_i, x_{ij}, x_{l_2 l_2})$ used in the formula are obtained from Kozak and Bogaerts.[1] v_i and l_2 represent the quantum numbers discussed in the previous part and d_i are the degeneracies of the main modes of vibration $(d_1, d_2, d_3) = (1, 2, 1)$.[1]

The values can be found in Appendix A1 and the results in Appendix A2. Only the levels needed for the further calculations and code will be calculated (i.e. the ones related to vibrational dissociation of the CO_2-molecule).

C. Intermezzo: V-V and V-T exchange

We now define and discuss the various mechanisms of vibrational exchanges considered in this work: vibrational-translational (V-T) and vibrational-vibrational (V-V) exchanges. A V-T-transition occurs when two molecules collide and one of them will undergo a transition in vibrational mode, i.e., gain or lose energy from/to the translational mode. It can be represented by:

$$M(v) + M \overset{k}{\leftrightarrow} M(v') + M, \tag{3}$$

where M is a generic molecule (e.g. CO_2) and v and v' represent different quantum numbers in which v' represents the quantum transitions like v-1, but can be an also multi-quanta transition. In a V-V-reaction both collision partners will be vibrationally excited, and during a collision they will exchange vibrational energy, so therefore one molecule will gain vibrational energy, while the other one will lose vibrational energy, represented by:

$$M(v) + M(w) \overset{k}{\leftrightarrow} M(v') + M(w') \tag{4}$$
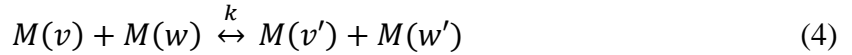
D. CO₂ conversion in plasmas[18]

From a practical point of view, all the research involving CO_2 conversion in plasma has one common task: increasing the energy efficiency associated with the decomposition process, while keeping the dissociation rate at reasonably high level. In this section we overview the various mechanisms related to the CO_2 conversion process. The first step in CO_2 endothermic decomposition is:

$$CO_2 + M \rightarrow CO + O + M \qquad \Delta H = 5.5 \; eV/mol \tag{5}$$
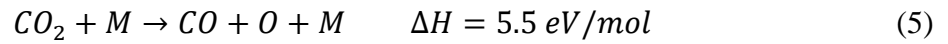
The oxygen can then continue to react with carbon dioxide

$$CO_2 + O \rightarrow CO + O_2 \qquad \Delta H = 0.3 \; eV/mol \tag{6}$$
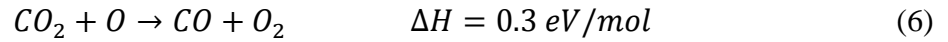
This gives a total reaction of

$$2 \; CO_2 \rightarrow 2 \; CO + O_2 \qquad \Delta H = 5.9 \; eV/mol \tag{7}$$

Or in reduced form

$$CO_2 \rightarrow CO + \frac{1}{2} O_2 \qquad \Delta H = 2.9 \; eV/mol \tag{8}$$
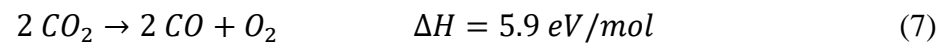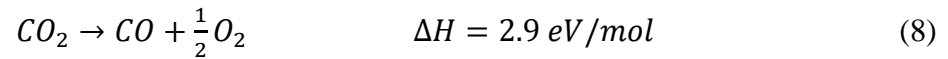
The efficiency of the process can be calculated with the obtained dissociation enthalpy

$$\eta = \frac{\Delta H}{E_{CO.}}, \tag{9}$$

where E_{CO} is the actual energy cost of one CO molecule produced in the plasma reactor. There are many channels and ways that can cause CO_2 to be dissociated: (electron impact) vibrational excitation, electronic excitation and dissociative attachment of electrons as well as electron impact ionization followed by dissociative recombination.

As already mentioned before, it was proven that vibrational excitation is the most effective channel for CO_2 dissociation in plasma. Electrons at an electron temperature of T_e = 1-2 eV are very efficient in transferring energy to mostly the asymmetric excitation mode. More than 95% of the energy can be transferred. The vibrational energy is in addition most effective in stimulating the dissociative reactions. For the dissociation, the vibrational energy required is also lower than for dissociation using electronic excitation and equals the energy of the C=O bond (5.5 eV). Of all the vibrational modes the asymmetric stretch is preferred the most, as a result of some special properties it contains. For instance, the V-T relaxation constants for the asymmetric stretch are lower than the ones for the symmetric stretching and bending modes. Additionally, the vibrational energy exchange (V-V) between the asymmetric stretch levels is very fast (faster than for the other vibrational modes). This leads to population of highly excited states for this mode.[18]

On the other side, CO_2 can also become dissociated through means of electronic excitation. This is a consequence of direct electron impact and when the energies are high, even electronically exited CO can be produced. This dissociation mechanism can become dominant in non-thermal plasmas with high reduced electric fields or when the plasma is obtained through degradation of very energetic particles as it is in the case of high-energy electron beams. This contributes to suppression of the vibrational excitation. Moreover, the maximum efficiency of this mechanism is still low (around 25%) due to some limitations. As mentioned before, with electronic excitation, more energy is required than for vibrational excitation. The required energy even exceeds the bond energy. This leads to energy losses. Furthermore, the fraction of energy transferred from the plasma electrons to the electronic channel is relatively low. At last, for the dissociation through electronic excitation to be relevant, relatively high electron temperatures (order of 10 eV and up) are required.

Another mechanism also including electrons is dissociative attachment. Here an electron will collide with CO_2, attach itself, causing dissociation of the molecule:

$$CO_2 + e \rightarrow CO + O^-$$ (10)

The oxygen ion can continue to react and cause the reverse reaction of (10) with CO or react with CO_2 producing CO_3.

$$O^- + CO \rightarrow CO_2 + e$$ (11)

$$O^- + CO_2 \rightarrow CO_3 + e \tag{12}$$

These reactions will limit the energy efficiency. The loss of an electron contributes to this as well. Nevertheless, the dissociative attachment is still an important mechanism due to creation of an ion and uptake of an electron and so influences the balance of charged particles. This way it contributes to sustaining the non-thermal discharge.

As last, a non-direct mechanism is discussed: ionization followed by dissociative electron-ion recombination. The latter is a neutralization mechanism; thus it recombines two charged particles into a neutral one. Ionization is a key process in the plasma, since plasma, an ionised gas, is sustained by it:

$$CO_2 + e \rightarrow CO_2^+ + e + e, \tag{13}$$
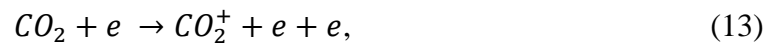
where reaction 13 represents direct ionization of CO_2. This can be followed by the recombination reaction:

$$CO_2^+ + e \rightarrow (CO_2)^* \rightarrow CO + O^* \tag{14}$$
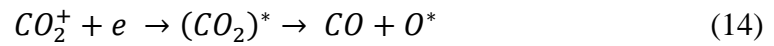
This reaction happens quite fast and plays a major role in molecular gasses like CO_2 (with reaction rates around 10^{-7} cm^3/s). The reaction is highly exothermic, and thus this energy contributes to the dissociation of the molecular ion. In a CO_2-plasma ionization can be the most important electron-impact conversion mechanism, due to relatively high cross sections (10^{-19} cm^3/s) in combination with the possibility of dissociation through recombination.[42]

2. The H₂O-molecule

A. General
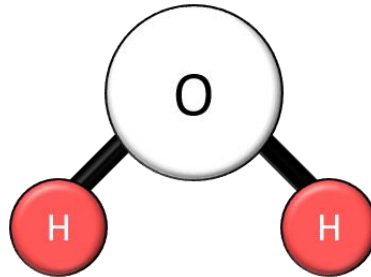
Figure 9: Schematic representation of the water molecule

Water is the essential component in life. It is in the oceans that our life started and without water we would not be able to survive. Moreover, water is also the most important greenhouse gas in the atmosphere. Water is not only important on earth, in the universe H_2O is even the third most abundant molecule (after H_2 and CO). Water is so important that our metric system is based on it, namely the melting and boiling points are used as basis for the Celsius-system, where they are set as 0° and 100°, respectively.

Water is a nonlinear triatomic molecule consisting of one oxygen atom and two hydrogen atoms (figure 9), giving it therefore a molecular weight of 18,01528 g/mol. The configuration of water is H-O-H, with an angle of 104.5° in between, thus causing water to be non-linear. Therefore, water has a permanent dipole moment (μ) of 1.8546 D along the symmetry axis of the molecule. The ionization energy of water is 12.621 eV, while the dissociation energy is 5.0992 eV. Since H_2O is a triatomic molecule it has 9 degrees of freedom (3N). It has three modes of vibration (3N – 6), three rotational modes and three translational modes.[43]

The vibrational modes consist of a symmetric stretch, bending and asymmetric stretch, noted as (v_1, v_2, v_3) (figure 10). The wavenumbers of these modes are 3656.7 cm^{-1}, 1594.8 cm^{-1}, and 3755.8 cm^{-1}. It is important to mention that only in special cases (like the CO_2-molecule), the modes are completely independent and so purely stretching or bending. In general, the modes are a combination of both. In H_2O, in contrast to the CO_2-molecule, all three modes are infrared and Raman active. The characteristic temperatures of the vibrations of H_2O are 5300 K, 2300 K, and 5400 K, accordingly to its high wavenumbers. Therefore, even at high temperatures (like 1500 K) most molecules will be in their vibrational ground state. In the next subchapter the vibrational levels will be calculated.[39]
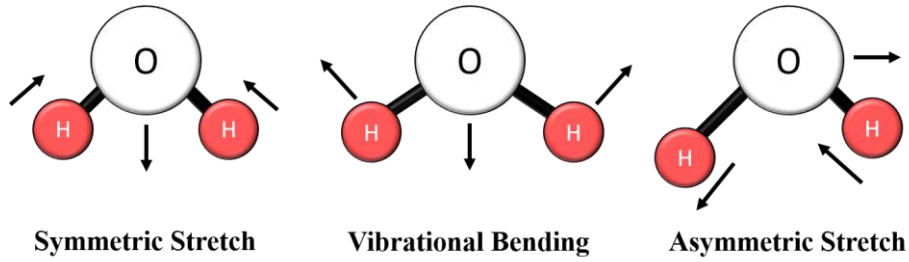
Figure 10: Schematic representation of the different vibrational modes of H₂O

Compared to the vibrational levels, the three rotational modes have characteristic temperatures of 40 K, 21 K, and 13 K, and are therefore fully excited. The rotational constants are 27.877 cm^{-1}, 14.512 cm^{-1}, and 9.285 cm^{-1}. Moreover, as a consequence of the small interlevel spacings, water molecules in the gas phase (at finite temperature) will be populated over a large range of rotational states. Due to its non-linearity, water has three different and non-zero moments of inertia, and is therefore an asymmetric top-rotor. Consequently, the rotational levels are a bit more complicated. Water has two separate sets of rotational energy levels, denoted by the Greek letter τ. Depending on the value of τ, the levels will belong to the para levels (if the value of τ is even) or the ortho levels (if the value of τ is odd). The formula to obtain τ is:

$$\tau = K' - K'', \tag{15}$$

where K' is the projection of J along the axis of least moment of inertia and K'' is the projection along the largest moment of inertia. The pseudoquantum number τ can have the values of:

$$\tau = J, J - 1, J - 2, \dots, -J \tag{16}$$

Therefore, the levels are noted as $J_{K'K''}$ or J_τ. It is also important to mention that transitions between the two sets of rotational states are not allowed and that neither photo-absorption nor electron impact can induce this transition. The only transitions that are allowed stem from the selection rule.

$$\Delta J = 0, \pm 1 \tag{17}$$

According to the selection rule (and so molecular symmetry) only para (even τ) states can be excited from the ground state $J_\tau = 0_0$. The levels up to J = 3 can be found in Table 1.[44]

Table 1: Rotational levels of H₂O. Note the small interlevel spacings

Para		Ortho	
J_τ	Energy (meV)	J_τ	Energy (meV)
0_0	0.000	1_{-1}	2.950
1_0	4.604	1_1	5.253

2_{-2}	8.690	2_{-1}	9.856
2_0	11.800	2_1	16.726
2_2	16.882	3_{-3}	16.956
3_{-2}	17.640	3_{-1}	21.495
3_0	25.578	3_1	26.304
3_2	35.363	3_3	35.387

B. Calculation of the vibrational levels

For simplicity the same approach as for the CO_2-molecule will be used, with the biggest difference that H_2O does not possess the special angular momentum quantum number and therefore the formula can be reduced to:

$$\frac{E_{H_2O}}{hc} = \sum_i \omega_i \left(v_i + \frac{d_i}{2}\right) + \sum_{j \geq i} x_{ij} \left(v_i + \frac{d_i}{2}\right)\left(v_j + \frac{d_j}{2}\right) \tag{18}$$

Also, it is important to mention that compared to the CO_2-molecule the v_2 bending mode is not double degenerate. The constants[45] can be found in Appendix A3 and the levels in Appendix A4.

B. Part 1: Building the Cross Section Set

Electrons are often considered to be the primary agents in plasmas. They are accelerated by the applied electric fields and give rise to a chemically-rich environment due to collisions with heavy particles, yielding excitation of internal degrees of freedom, dissociation and ionization. Therefore, the accurate knowledge of electron impact cross sections is of a special importance in gas discharge modelling. Cross sections are of critical importance for the calculation of (among other parameters) the electron energy distribution function (EEDF), which plays a key role in gas discharges, as it describes the probability density for an electron to have an energy ε.

In this part of the thesis we present the formulation required to build a set of electron cross sections for H_2O with interest for the modelling of CO_2-H_2O plasmas. These cross sections, compiled from different databases, are used as input data to different numerical codes, to obtain transport coefficients and collision rate coefficients. A more detailed discussion about the creation of the set can be found in Results and Discussion: Part 1.

1. Reviewing Cross Sections and Swarm Parameters

In order to propose the cross sections for electron collisions with H_2O, which will be used for the modelling of CO_2-H_2O plasmas, it is important to introduce the concepts of consistent and complete sets. A set is considered complete when it is able to describe the main electronic processes responsible for momentum and energy losses, including those yielding changes in the number of electrons, such as ionization. On the other hand, a set is consistent when it is able to reproduce measured values of swarm parameters, when used as input data to evaluate the EEDF from a Boltzmann solver.[46] The Boltzmann solvers used in this work are described below.

A complete and consistent set of cross sections is often obtained adopting a swarm-based procedure.[46] A swarm of charged particles is an ensemble (collection) of particles moving through the background gas under the influence of an external electric field.[47] Therefore, swarm parameters are parameters related to the transport of electrons (measured under an applied electric field). The parameters will be obtained from the LXCat database and Hasegawa et al.[48] Swarm parameters can be used to derive the cross sections, as well as to control the validity of the created set. The latter procedure starts with the collection of a set of cross sections from the literature, whose magnitudes are adjusted to improve the agreement between calculated and measured swarm data. Here it is important to mention that such procedure does not validate the cross section of each individual process nor it ensures the uniqueness of the whole cross section

set. As a consequence, multiple sets of cross sections can provide the right transport data. There are some ways to correct this, like obtaining more information about the relative magnitudes of the processes or putting several processes into one cross section.[49] The swarm parameters calculated in this work are the (i) electron reduced mobility and (ii) effective ionization Townsend coefficient, represented by μN and α/N - η/N, respectively.

Mobility (μ) is the parameter that describes the drift of particles (in this case in a plasma) in an external electric field E and is given by:[50]

$$\mu = \frac{|u|}{E} = \frac{q}{m * v_m},$$
(19)

where u represents the drift (the average velocity a particle gains from an electric field), q the electrical charge, m the mass and v_m the momentum transfer collision frequency. For electrons, this corresponds to the transport of mass and the conduction of electricity. A parameter closely related to mobility is diffusion D, since they are both related to the motion. Their relation is given by the Einstein relation:[50]

$$\mu = \frac{q * D}{k_B * T},$$
(20)

where T is the absolute gas temperature and k_B is the Boltzmann constant. On the other hand, the reduced Townsend coefficient/effective ionization Townsend coefficient is the difference between the Townsend ionization coefficient α (total number of electrons created per unit length) and the Townsend attachment coefficient η (total number of electrons lost per unit length) divided by the gas density N.

The calculations follow the expressions:[51]

$$\mu N = -\frac{\sqrt{2e/m_e}}{3} \int_0^\infty \frac{\varepsilon}{Q} \frac{\delta f_0}{\delta \varepsilon} d\varepsilon$$
(21)

$$\frac{a}{N} - \frac{\eta}{N} = \frac{K_{ion} - K_{att}}{u_e}$$
(22)

where e is the electron charge, m_e is the electron mass, ε is the electron energy, Q is the collision cross section, f_0 is the EEDF, K_{ion} is the ionization coefficient, K_{att} is the attachment coefficient and u_e is the electron drift velocity. These swarm parameters are calculated over a large range of reduced electric fields, E/N =10^{-2} – 10^3 Td (where E is the electric field and N is the gas number density; 1 Td = 10^{-17} V cm^2). The calculations are performed at room temperature (i.e T = 300 K). Energy sharing after ionization is considered equal. For the

calculations, the growth model (related to the effects of production or loss of electrons in ionization or attachment) Steady-State Townsend (SST) was chosen, which is based on exponential spatial growth. This means exponential growth of the electron current between the electrodes.[46]

2. Simulation Tools

The main simulation tool used in this work for the calculation of swarm parameters and EEDF is BOLSIG+.[51] This simulation tool is a free and user-friendly computer program for the numerical solution of the Boltzmann equation for electrons in weakly ionized gases in uniform electric fields. The Boltzmann equation can be written as:

$$\frac{\partial f}{\partial t} + v * \nabla f - \frac{e}{m_e} E * \nabla_f f = C[f], \tag{23}$$

where f is the electron distribution in six-dimensional phase space, *v* are the velocity coordinates, E is the electric field and *e* the elementary charge. The right part of the equation represents the rate of change in the electron distribution due to collisions. Note that in this equation we consider a space with six dimensions or degrees of freedom where each unique point is represented by a state. Therefore, six coordinates are needed to specify the location in this space. The total space contains all possible states.

To obtain solutions from the Boltzmann equation, some simplifications are needed. In this case, the first assumption that is made is that the electric field and collisions are uniform on the scale of the collisional mean free path (average distance travelled by a particle between two collisions). If spherical harmonics are used, f becomes dependent on four coordinates: time t, the magnitude of the field direction *v*, the angle between the velocity and the field direction θ, and the position along this direction z. Another simplification is that the time-dependence is considered steady state. This results in the electric field and electron distribution being stationary. For the angular dependence, the two-term approximation is used. Here, the electron distribution is expanded in terms of Legendre polynomials (solutions of the Legendre differential equation) and then used to construct the equations from the expansion coefficients by filling them in into the Boltzmann equation. The term "two-term approximation" comes from the fact that only two expansion terms are used. This gives lower precision, but is good enough for lower values of E/N.[51]

In addition to the BOLSIG+ simulation tool, the LoKI code was used for comparison purposes. The LoKI code is an in-house simulation tool at N-PRIME[52,53] that couples two main calculation blocks to solve: (i) the homogeneous two-term electron Boltzmann equation (for a pure gas or a gas mixture, including first and second-kind collisions, as well as electron-electron collisions); (ii) the system of zero-dimensional (volume averaged) rate balance equations for the most relevant charged and neutral species in the plasma. In this work, only part (i) has been used, in order to validate the swarm parameters calculated through the BOLSIG+ tool.

3. EEDF

As we stated before, the electron energy distribution function is an important parameter and can be obtained by solving the Boltzmann equation (23). This function is necessary to compute reaction rates for electron collisions and transport properties. Note that often this EEDF is assumed to follow a Maxwellian shape in thermal equilibrium, which means that it can be evaluated by electron temperature T_e. In this case, the Maxwellian distribution is given by:[18]

$$f(\varepsilon) = A * \exp\left(\frac{-\varepsilon}{k_B * T_e}\right), \tag{24}$$

$$with\ A = 2 * \sqrt{\frac{\varepsilon}{\pi(k_B * T_e)^3}}. \tag{25}$$

This leads to an electron mean energy of:

$$\langle\varepsilon\rangle = \int_0^\infty \varepsilon f(\varepsilon)d\varepsilon = \frac{3}{2}T_e. \tag{26}$$

However, in many cases, deviations occur and non-thermal plasma often possess non-Maxwellian distributions. Note that, when the EEDF is calculated from the solution of the Boltzmann equation (as it happens in this work), the distribution follows a non-Maxwellian shape.[51] At last, as a side note, the EEDF is very hard to measure experimentally, so again this is a confirmation for the added value of simulations.

4. Calculation of the Rotational Populations

In water the rotational levels are broadly populated at room temperature, therefore for correct calculations of swarm parameters, the relative populations are required. These will be later used in calculations for the LoKI code and will be calculated up to J =3. These relative populations will be calculated using the Boltzmann distribution:

$$\frac{N_J}{N} = \frac{g_y exp\left(-\frac{E_J}{k_b T g}\right)}{\sum_{J=0}^{3} g_y^J exp\left(-\frac{E_J}{k_b T g}\right)},$$

(27)

where N_J is the number of particles in level J and N the gas density, g_y the weight of the level and E_J the energy of the level J (calculated according to Tennyson et al.[44]). Note that in the case of water, we must take into account that a rotational level J is split up into para and ortho levels, therefore the populations of J will be a sum of the populations of both sets of levels belonging to one particular J. The relative weights for the para and ortho levels are one and three.[40]

The results for 300 K can be found in table 2.

Table 2; Populations of the rotational levels of H_2O.

Rotational Level J	Population (%)
0	5.47
1	32.49
2	30.05
3	31.99

C. Part 2: The kinetic model

Here we discuss the formulation used to describe the vibrational kinetics in CO_2-H_2O discharges. For this purpose, we have used two simulation tools: the kinetic model developed by Kozak and Bogaerts[1] and further optimized by Berthelot and Bogaerts[54,55] and the state-to-state approach developed by Silva et al.[2] The contribution of this work is related to the addition of H_2O to these models and is discussed as well in the end of the section.

1. The model of Kozak and Bogaerts[1,13]

The calculations will be performed by the Fortran 90-module, called ZDPlasKin.[56] This is a zero-dimensional solver, and thus, as a result of the zero dimensionality, the plasma will be assumed to be homogenous, meaning the model will not account for diffusion and convection. The changes in concentration will only be a function of time. Therefore, only the mass conservation equations for every particle and the Boltzmann equation will be solved. Therefore, ZDPlasKin[56] will follow the time evolution of species densities and gas temperature. The mass conservation equations for every particle are:

$$\frac{dn_s}{dt} = \sum_{j=1}^{jmax} Q_{sj} = \sum_{j=1}^{jmax} R_j \left[a_{sj}^R - a_{sj}^L \right], \tag{28}$$

$$R_j = k_j \prod_l n_l , \tag{29}$$

where n_s is the density of the species s, Q_{sj} is the source term for reaction j of the species s, a_{sj}^R and a_{sj}^L represent the stoichiometric coefficients on the right and left site, respectively, of species s for reaction j. R_j is the reaction rate and k_j the reaction rate coefficient.

The gas temperature can be chosen to remain constant or can vary with the time. In the latter situation the temperature would be calculated by:[13]

$$N \frac{\gamma k_B}{\gamma - 1} \frac{dT_{gas}}{dt} = P_{el} - \sum_{j=1}^{jmax} \Delta H_j * R_j - P_{ext} , \tag{30}$$

where N is the total gas density and γ is the specific gas heat ratio. P_{el} is the power transferred from the electrons to the heavy particles as a consequence of elastic collisions and ΔH_j the enthalpy/heat released or consumed during reaction j. In the code, cooling due to heat conduction will be also accounted for by using the radial, that can be calculated as:[13]

$$P_{ext} = \frac{8\lambda}{R^2}\left(T_{gas} - T_{wall}\right),$$
(31)

$$\lambda = \left(0.071 T_{gas} - 2.33\right) \times 10^{-15},$$
(32)

where λ (W cm^{-1} K^{-1}) is the thermal gas conductivity of CO_2 and R the tube radius.

To run ZDPlasKin, different smaller codes and files are needed. These submodules will work together and are shown in figure 11.[56] The files that should be provided by the user are kinet.inp, the user code and de Bolsig+ datafile.
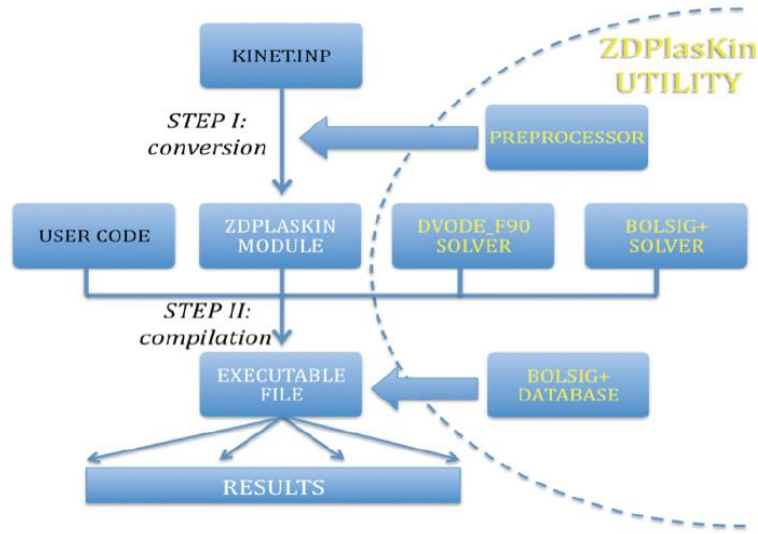
Figure 11: Schematic overview of ZDPlasKin -The kinet.inp will be converted to a fortran module using the pre-processor. Next, the master code containing the used ZDPlasKin routines is compiled using gfortran. This creates an executable file that when run will provide the output files.[56]

The main master code will provide the commands for the calculations and will call the needed ZDPlasKin routines. It will as well contain the geometry of the reactor, that can be changed using an input file read by the master code. The reactor geometry used is a surfatron MW plasma, where the gas flow is moving through a cylindrical discharge tube (cooled to room temperature) and will be passing through a plasma (region) that is formed using microwaves that are guided perpendicular to the tube (figure 12). As a result of the 0D-model all variables are taken as uniform in the radial direction and diffusion and heat conduction are neglected along the reactor axis. By using the 0D approximation the reaction kinetics and gas flow along the reactor axis will be described, creating a pseudo 0D-model.[54] Using the conservation of mass flow rate, the velocity v of a volume in the tube can be calculated:

$$v = \frac{Q_m}{\rho * A} = \frac{Q_m}{\sum_s n_s M_s * \pi R^2} \quad ,$$
(33)

where Q_m is the mass flow rate, ρ is the mass density of species s (calculated from the number density m and the mass M) and A the cross section area. Since velocity is related to time and position, the time-dependence can be converted into position-dependence. In this case the parameters will be therefore expressed as a function of the axial coordinate z. The master code will also consider the power density profile, which is in this case triangular:[54]

$$Q_{MW}(z) = \left(1 - \left|\frac{z-(z_p+{}^L/_2)}{{}^L/_2}\right|\right) * P_{max} \; if \; z_p \leq z \leq z_p + L \tag{34}$$

$$P_{MW} = A \int_{z_p}^{z_p+L} Q_{MW}(z)dz = \frac{AL}{2} Q_{max} \tag{35}$$

In any other case, the axial coordinate is outside the plasma and thus Q_{MW} is zero. In the formula z_p is the beginning of the plasma, L the length of the plasma. Using Q_{MW} the total deposited power P_{MW} can be calculated, where Q_{max} is the maximum power deposition density. If divided by two, the latter also gives the mean power deposition density.
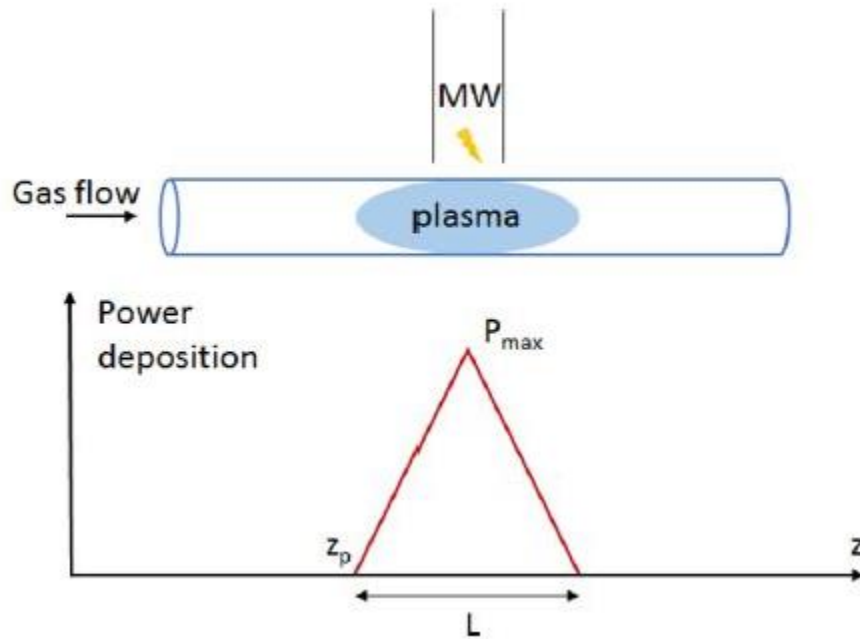
Figure 12: Schematic overview of the reactor geometry and the deposited power. L represents the length of the plasma. [54]

For this master thesis, the geometry was not changed, since the focus is on the reactions. The master code was only changed to also accommodate H_2O, thus including hydrogen-containing species (see further in section 4). The set-up used was according to Berthelot et al.[54] at a temperature of 300 K and a pressure of 300 mbar.

As already mentioned, the asymmetric mode is the most important mode to be included in the CO_2 model. Since the dissociation energy is 5.5 eV all asymmetric levels until that limit should be included. This corresponds to including all (0 0 n) levels up to (0 0 21). From the other two modes only the lower lying levels will be included, since plasma electrons provide mostly excitation in the low vibrational levels. Given the fermi resonance between some v_1 and v_2 modes, the four lowest lying levels of the bending mode will be included and so by implication also the resonant symmetric levels.
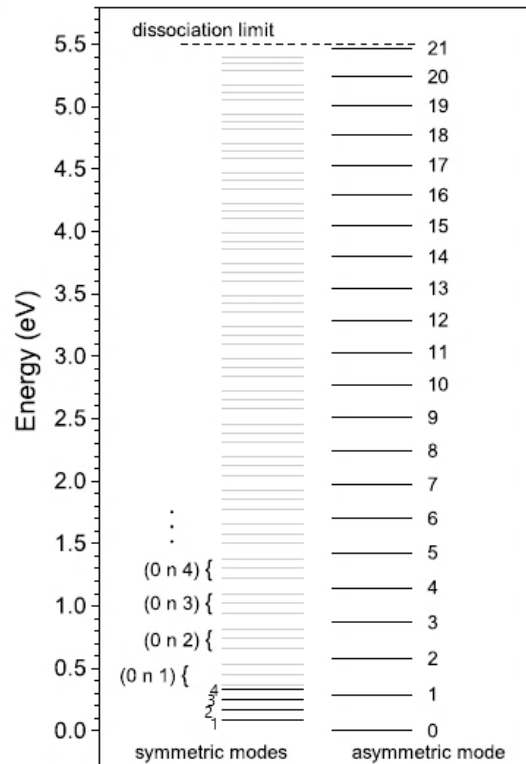
Figure 13: A schematic representation of the vibrational levels of CO_2 up to the dissociation limit, included in the model of Kozak and Bogaerts[1]

2. The model of Silva et al.[2]

The model of Silva et al.[2] was developed to describe the time evolution of CO_2 vibrational levels during the plasma pulse of a DC glow discharge and its afterglow, at pressures of about 5 Torr, discharge currents around 50 mA for a plasma pulse of 5 ms on-time. The model couples the electron Boltzmann equation to the rate balance equations for the first 72 individual vibrational levels, corresponding to all vibrational levels of v_1 up to 2 and v_2 and v_3 up to 5.

They consider electron impact reactions (e-V), vibrational-translational (V-T) and vibrational-vibrational (V-V) exchanges and radiation losses ($h\nu$) according to the following system:

$$\frac{dn_v}{dt} = \left(\frac{dn_v}{dt}\right)_{e-V} + \left(\frac{dn_v}{dt}\right)_{V-T} + \left(\frac{dn_v}{dt}\right)_{V-V} + \left(\frac{dn_v}{dt}\right)_{hv}, \tag{36}$$

where n_v represents the concentration of each vibrational level. As input for this model they have considered the gas pressure, gas temperature and the concentrations of the various vibrational states at the beginning of the on-time of the pulse or the beginning of the afterglow. These concentrations were obtained using the vibrational distribution (see section 3) and experimental values[57] of T_{12} and T_3. These temperatures correspond to the population of the symmetric stretch and bending modes (taken together here due to the Fermi-coupling) and asymmetric stretch mode, respectively. As input for the gas temperature, an experimentally obtained profile is used. The experimental set-up used for the validation of this model can be found in Klarenaar et al.[57]

In this work, based on the model of Silva et al.[2], we will investigate the influence of water in CO_2 discharges. Note, however, that this part of the study was limited to the analysis of the plasma afterglow in which electron impact processes are not considered. In other words, we have not considered the first term in (36). In regards of water addition, we have included one additional term to (36) related to V-T mechanisms between CO_2 and H_2O. This allows studying the time-resolved evolution of vibrational temperatures or vibrationally excited CO_2 levels densities for different percentages of water.

3. Distributions of Populations[18]

At this point, we would like to emphasize possible vibrational distributions taken into account in the kinetic models presented above. More especially, two types of vibrational distributions are considered in this work: Boltzmann and Treanor. Their description can be found below.

- *Boltzmann distribution*

The most commonly known distribution is the Boltzmann distribution, that gives a linear logarithmic correlation between the (energy of) levels v and the corresponding number densities n_v and is given by:

$$n_v = n_0 \frac{g_v}{g_0} exp\left(-\frac{E_v}{T_v}\right), \tag{37}$$

where n_0 is the ground state density, $g_{v(0)}$ is the statistical weight of the vibrational (ground) state, E_v is the vibrational energy of the level v and T_v is the vibrational temperature.

- *Treanor distribution*[58]

In equilibrium, the distributions of diatomic molecules can be expressed by the Boltzmann distribution, but this is not always the case. In non-equilibrium situations, and when vibrational excitation in non-thermal plasma is faster than vibrational–translational (V-T)-relaxation, and when the molecules can be represented as anharmonic oscillators, deviations from the traditional Boltzmann distribution occur. The acquired distribution can then be represented by the Treanor distribution given by:

$$n_v = n_0 exp\left(-\frac{vE_1}{T_v} + \frac{vE_1 - E_v}{T_g}\right), \tag{38}$$

The densities of the levels are a function of both the vibrational temperature T_v and the gas temperature T_g. E_1 represents the energy of the lowest vibrational level. This distribution leads to the higher levels being more populated.

Important to mention is that both the Boltzmann and Treanor distributions are just approximations that also tend to fail at higher vibrational numbers. The Treanor approximation also does not take into account the influence of dissociation and V-T-transfers, resulting in an overestimation of the higher vibrational levels.[54]
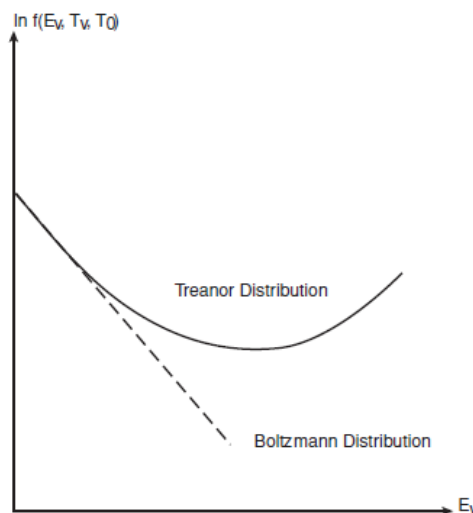
Figure 14: A simple comparison of the Boltzmann and Treanor distribution[18]

4. Inclusion of Water: Reactions and Species

Having described the two kinetic models, we present now the contribution of this work related with the inclusion of H_2O in both codes. This includes: (i) V-T-reactions associated with the quenching of vibrationally excited CO_2-states by H_2O, and (ii) V-T-reactions connected with the quenching of vibrationally excited H_2O states by H_2O and CO_2. This involves the inclusion of H_2O vibrationally excited states to the code, which already includes V-T and V-V-transfer reactions of CO_2 with the included neutrals (like CO_2, O_2 and CO), ion-neutral and ion-ion reactions, electron impact reactions, electron attachment and electron-ion recombination reactions and reactions with neutrals. A more extended overview can be found in the paper of Kozak and Bogaerts.[1] Thus, no new reactions involving collisions between CO_2 species are added to the previously mentioned kinetic models. An overview of the new species of water added to the code is given below. The extra added species are a result of the dissociation of water.

Added Species of Water	Extra Added Species
H_2O	H_2, OH, H
$H_2O(100)$, $H_2O(010)$, $H_2O(001)$, $H_2O(020)$	
H_2O^+	H^-

All the reaction rates coefficients used/calculated in this work (see below) follow the expression:

$$k = X \, \text{Exp}\left[A + BT^{1/3} + CT^{2/3}\right], \tag{39}$$

where A, B and C are fitting constants (listed in Appendix A5) and X is a multiplication factor with the value of (Avogadro's number)$^{-1}$, used in order to express the rate coefficient in units of $cm^3 \cdot s^{-1}$. The reactions and rate coefficients were obtained from Blauer[59] and the calculated values at 300 K will be listed below.

CO$_2$-H$_2$O V-T-reactions

Reaction	k (cm^3·s^{-1})
$CO_2(01^10) + H_2O \rightarrow CO_2(00^00) + H_2O$	$9.85 \cdot 10^{-12}$
$CO_2(02^00, 10^00) + H_2O \rightarrow CO_2(01^10) + H_2O$	$1.33 \cdot 10^{-12}$

$$CO_2(02^00, 10^00) + H_2O \rightarrow CO_2(00^00) + H_2O \qquad\qquad 6.94\cdot10^{-13}$$

$$CO_2(03^10, 11^10) + H_2O \rightarrow CO_2(02^00, 10^00) + H_2O \qquad\qquad 3.99\cdot10^{-11}$$

$$CO_2(03^10, 11^10) + H_2O \rightarrow CO_2(01^10) + H_2O \qquad\qquad 1.97\cdot10^{-15}$$

$$CO_2(00^01) + H_2O \rightarrow CO_2(02^00, 10^00) + H_2O \qquad\qquad 1.24\cdot10^{-13}$$

$$CO_2(00^01) + H_2O \rightarrow CO_2(03^10, 11^10) + H_2O \qquad\qquad 2.31\cdot10^{-13}$$

$$CO_2(00^01) + H_2O \rightarrow CO_2(01^10) + H_2O \qquad\qquad 1.81\cdot10^{-15}$$

$$CO_2(04^00, 12^00, 20^00) + H_2O \rightarrow CO_2(00^01) + H_2O \qquad\qquad 8.80\cdot10^{-16}$$

$$CO_2(04^00, 12^00, 20^00) + H_2O \rightarrow CO_2(03^10, 11^10) + H_2O \qquad\qquad 5.96\cdot10^{-11}$$

$$CO_2(04^00, 12^00, 20^00) + H_2O \rightarrow CO_2(02^00, 10^00) + H_2O \qquad\qquad 1.75\cdot10^{-15}$$

H_2O-H_2O and H_2O-CO_2 V-T-reactions

Reaction	$k\ (cm\cdot s^{-1})$
$H_2O(010) + H_2O \rightarrow H_2O(000) + H_2O$	$5.98\cdot10^{-11}$
$H_2O(020) + H_2O \rightarrow H_2O(010) + H_2O$	$1.19\cdot10^{-10}$
$H_2O(001) + H_2O \rightarrow H_2O(000) + H_2O$	$5.15\cdot10^{-17}$
$H_2O(100) + H_2O \rightarrow H_2O(000) + H_2O$	$5.87\cdot10^{-14}$
$H_2O(001) + H_2O \rightarrow H_2O(100) + H_2O$	$8.21\cdot10^{-12}$
$H_2O(010) + CO_2 \rightarrow H_2O(000) + CO_2$	$5.00\cdot10^{-14}$
$H_2O(020) + CO_2 \rightarrow H_2O(010) + CO_2$	$1.01\cdot10^{-13}$
$H_2O(001) + CO_2 \rightarrow H_2O(000) + CO_2$	$2.29\cdot10^{-20}$
$H_2O(100) + CO_2 \rightarrow H_2O(000) + CO_2$	$3.51\cdot10^{-19}$
$H_2O(001) + CO_2 \rightarrow H_2O(100) + CO_2$	$1.40\cdot10^{-11}$

Note that all the presented rate coefficients correspond to forward processes. For the reverse reaction rate coefficients k' we use detailed balance according to:

$$k' = k * exp\left(-\frac{\Delta H}{k_b T}\right), \qquad\qquad (40)$$

where ΔH is the energy released/absorbed during the reaction, k_b the Boltzmann constant and T the temperature.

5. The Schwartz, Slawsky, and Herzfeld (SSH) Theory and Scaling

Since the data found in literature is limited for higher levels, we use scaling methods to obtain additional rate coefficients for higher (0 0 n) levels (up to n=21, the dissociation limit of CO_2).

The reactions that will be scaled, are the following:
1. $CO_2(00^01) + H_2O \rightarrow CO_2(01^10) + H_2O$
2. $CO_2(00^01) + H_2O \rightarrow CO_2(02^00, 10^00) + H_2O$
3. $CO_2(00^01) + H_2O \rightarrow CO_2(03^10, 11^10) + H_2O$

More in general, these reactions are:
1. $CO_2(00^0n) + H_2O \rightarrow CO_2(01^1(n-1)) + H_2O$
2. $CO_2(00^0n) + H_2O \rightarrow CO_2(10^0(n-1)) + H_2O$
3. $CO_2(00^0n) + H_2O \rightarrow CO_2(11^1(n-1)) + H_2O$

Since the resulting levels are assumed to be depopulated quickly through V-T-relaxation, they are assumed to be in thermal equilibrium with the asymmetric levels and thus the following reaction for n > 1 is obtained:[1]

$$CO_2(00^0n) + H_2O \rightarrow CO_2(00^0(n-1)) + H_2O \tag{41}$$
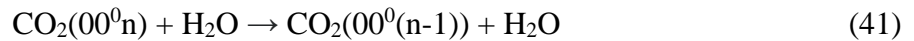
The resulting rate coefficient is then given by $k_{total} = k_1 + k_2 + k_3$. Note that in the Kozak and Bogaerts kinetic code[1], the reaction 41 will be included. However, for the Silva at al.[2] model, the separate reactions will be added.

For the scaling, the method of Schwartz, Slawsky, and Herzfeld, i.e., the SSH theory, was used.[1,60] The SSH theory is part of the first order perturbation theories (FOPT) and can provide relatively simple expressions for the state specific relaxation rates. The assumption made here is that strong, short-range, repulsive forces are effective in producing vibrational transitions. The biggest drawback is that one needs to be cautious when using the SSH theory for high temperatures or quantum levels due to the fact that the SSH theory is known to overestimate the vibrational transition probabilities in those cases.[2]

The same scaling strategy for V-T reactions will be used as Kozak and Bogaerts applied:[2]

$$k_{n,n-1} = k_{1,0} Z_n \frac{F(\gamma_n)}{F(\gamma_1)}, \tag{42}$$

where k is the rate constant for the V-T-relaxation, n the vibrational level of the molecule and Z is the scaling factor that can be expressed as:

$$Z_n = n \frac{1-x_e}{1-nx_e}, \tag{43}$$

in which x_e is the anharmonicity of the energy levels and is given by:

$$x_e = \frac{1 - {\Delta E_n}/{E_1}}{2*\left(n - {\Delta E_n}/{E_1}\right)}, \tag{44}$$

$$and \quad \Delta E_n = E_n - E_{n-1}, \tag{45}$$

where E is the energy of the given level.

Furthermore, the function F is given by:

$$F(\gamma) = \frac{1}{2}\left[3 - exp\left(-\frac{2}{3}\gamma\right)\right] exp\left(-\frac{2}{3}\gamma\right), \tag{46}$$

$$with \; \gamma_n = \frac{0.32\Delta E}{\alpha}\left(\frac{\mu}{T_g}\right)^{1/2}, \tag{47}$$

where the parameter γ_n is a measure of the adiabaticity (the amount of energy transferred). To calculate this parameter, the reduced mass $\mu = {m_1 m_2}/{m_1 + m_2}$ of the colliding species, and the value of the parameter for the exponential repulsive potential between the colliding species α, are needed. α can be calculated through:

$$\alpha = \frac{17.5}{r_0}, \tag{48}$$

here r_0 is the radius, or the distance at which the Lennard-Jones potential is zero (V = 0):

$$V(r) = 4 \in \left[\left(\frac{r_0}{r} \right)^{12} - \left(\frac{r_0}{r} \right)^{6} \right], \tag{50}$$

where r is the distance between the particles and $\in$ is the depth of the well. Here the calculations will be done for the CO_2-H_2O collisions. In this case r_0 is 3.60 Å.[61]

The results can be found in section Results and Discussion Part 2.

Chapter 3: Results and Discussion

A. Part 1: Finding the Cross Section Set

The first part of this research was focused on finding good cross sections for the electron impact reactions with water. As mentioned before, to begin the process of creating the dataset, the online database LXCat was consulted.

Different species can be found in LXCat, but the focus here is on water, since this is the new species added to the existing codes and models from the University of Antwerp and IST Lisbon. For water, five sets were available: Triniti, Itikawa, Hayashi, Morgan and Phelps (another set of Quantemol was also available but included only one reaction). Among these sets, only two – Triniti and Itikawa – were initially used. The other three lacked important rotational reactions and could therefore provide good results when used on Bolsig+. It is also worth mentioning that Phelps' cross sections range was too small and the cross sections were incomplete, so they were not used in building the sets.

To begin with, a basis set was chosen. This is a set that already has cross sections that can be run on Bolsig+ and gives quite good results in comparison with the experimental swarm parameters. Hereafter, the set was optimized and fine-tuned to include extra reactions and give a good overlap with the experimental swarm parameters. Unfortunately, as said above, only two sets were complete enough to run.

1. Comparing Triniti and Itikawa

Here we start with the comparison of swarm parameters calculated from two different sets of cross sections: Triniti and Itikawa. The results (reduced mobility and Townsend coefficient) are shown in figure 15. These results are compared with the experimentally measured data from Hasegawa et al.[48] For the reduced mobility (see figure 15a), none of the sets gives a good overlap. The experimental curve reaches its maximum ($1.22 \cdot 10^{24}$ $m^{-1}s^{-1}V^{-1}$) at 120 Td and then continues to lower values onwards. For the Itikawa set, the curve does not change significantly as a function of the reduced electric field. The curve has a flat slope, apart from the beginning, where it shows a small increase in values up to $1.13 \cdot 10^{23}$ $m^{-1}s^{-1}V^{-1}$. The calculated reduced mobility for the Triniti set shows a better agreement with the experimental data, although the values are too high. The maximum can be found at $1.72 \cdot 10^{24}$ $m^{-1}s^{-1}V^{-1}$ at 92 Td. However, compared to the Itikawa values, the shape of the curve is very similar to the experimental data.

Therefore, for the reduced mobility, the Triniti data set is favoured. Worth mentioning is that the Itikawa set contains separate cross sections for the different rotations, and since the populations of each level cannot be easily included in Bolsig+, this can also cause differences in the results. Later on, this will be taken into account to test the optimized datasets with a more advanced LoKI code from the IST research group. The Triniti set includes only one overall rotational cross section, so this problem does not occur in the calculations with this set.
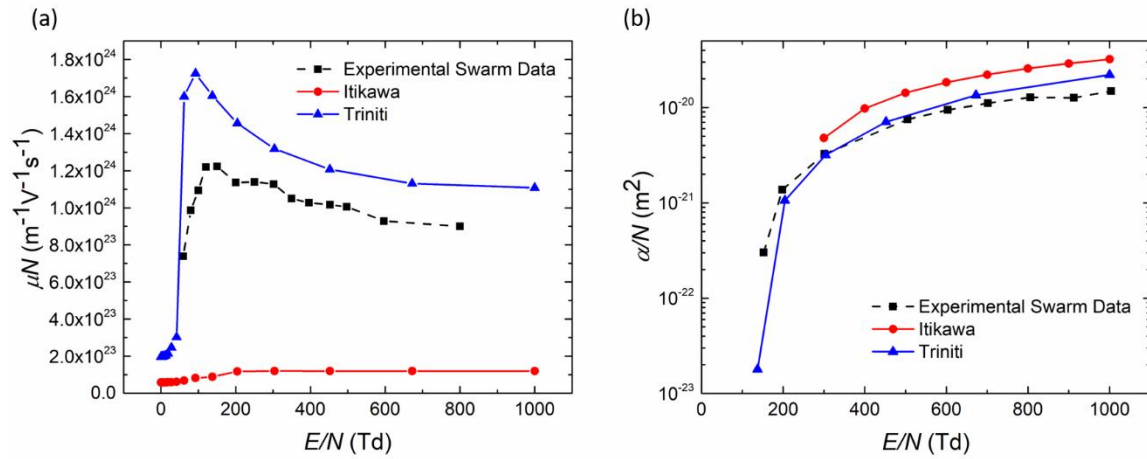
Figure 15: Comparison of the calculation results with the set of Itikawa and Triniti with experimental swarm data, for reduced mobility (a) and Townsend coefficient (b)

For the Townsend coefficient (see figure 15b) the experimental curve goes up from $3 \cdot 10^{-22}$ m^2 to around $1.28 \cdot 10^{-20}$ m^2. Both the calculated curves from the Triniti and Itikawa sets have the same shape. However, the Itikawa set reaches higher, up to $3 \cdot 10^{-20}$ m^2, while the Triniti curve is closer to the experimental values. Between 300 Td and 400 Td it overlaps with the experimental curve, but it continues to rise stronger than the experimental curve, and because of that it will end higher than the experimental one at around $2.21 \cdot 10^{-20}$ m^2. Nevertheless, the calculated curve from Triniti shows a better overlap with the experimental curve and therefore will be preferred.

From these first results we can conclude, from both reduced mobility and Townsend coefficient, that the Triniti set provides better results. Consequently, the Triniti set will be chosen as a base set to be optimized. The Itikawa set, however, contains some interesting reactions and cross sections and will be used to complete the Triniti set.

2. Overview of the Triniti Cross Section Set

A brief overview of the cross sections that are part of the Triniti set will be given (figure 16). The original Triniti set is derived from calculations of the EEDF software package for calculations of electron energy distribution function developed by Prof. Napartovich et al.[62] No paper was found including these cross sections, since it was posted straight into the database. The EEDF software can be obtained there as well.
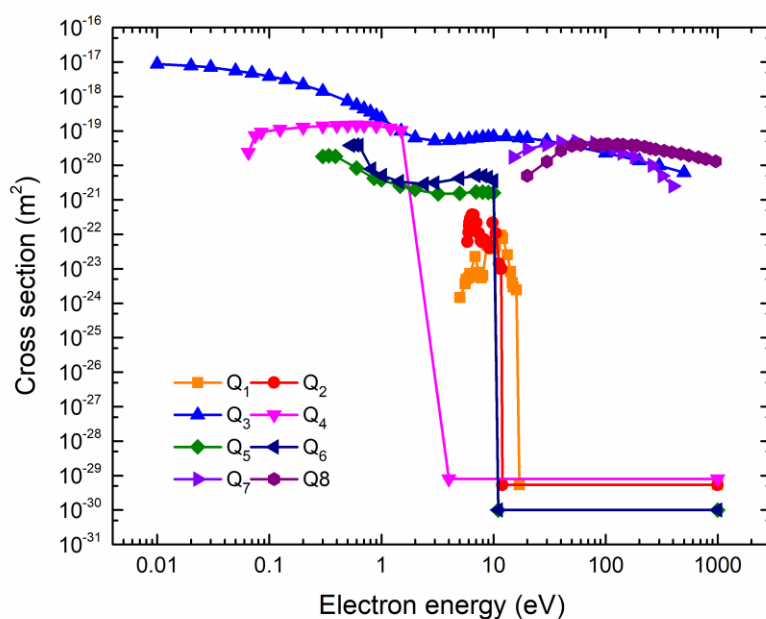
Figure 16: Cross sections included in the Triniti set

Reaction		Number
Dissociative Attachment	$e + H_2O \rightarrow H_2 + O^-$	Q_1
Dissociative Attachment	$e + H_2O \rightarrow OH + H^-$	Q_2
Effective Momentum Transfer	$e + H_2O \rightarrow e + H_2O$	Q_3
Excitation	$e + H_2O \rightarrow e + H_2O_{Rot}$	Q_4
Excitation	$e + H_2O \rightarrow e + H_2O(010)$	Q_5
Excitation	$e + H_2O \rightarrow e + H_2O(100,001)$	Q_6
Dissociation	$e + H_2O \rightarrow e + H + OH$	Q_7
Ionization	$e + H_2O \rightarrow e + E + H_2O^+$	Q_8

It should be noted that the effective cross sections are a sum of the elastic and inelastic cross sections. Therefore, the code will obtain the elastic cross section by subtracting the inelastic from the effective. The vibrational stretch cross sections are grouped together, since the symmetric and asymmetric levels lay very close (0.453 eV and 0.466 eV) and it is not possible to separate them with the present resolution.[63] The two attachment processes are also the two most important ones.[64]

3. Understanding the Influence of the Cross Sections

In this part of the work we performed various tests with Bolsig+ in order to understand the influence of each cross section on the shape of the calculated swarm parameters. This is an intermediate step in order to gain some insight in the influence of each individual cross section on the calculated swarm parameters. Consequently, this step is often not reported in papers, but it was chosen to do so in this master thesis, to give a complete overview of the process behind the development of a cross section set. The first step was to find a good range to work with. Since the uncertainties of cross sections of water are in general between 10% and 20% (sometimes up to 30%, however it has to be noted that the uncertainties are not always provided),[43] it was chosen to evaluate even larger uncertainties, to be certain that the cross sections have been changed significantly. Therefore, as an illustration of the effects, it was chosen to multiply all cross sections with a factor of 2. To obtain this and the following results, more than 20 sets were created. Figure 17 shows the results for the reduced mobility and Townsend coefficient, obtained by multiplying each cross section Q separately by a factor of 2.
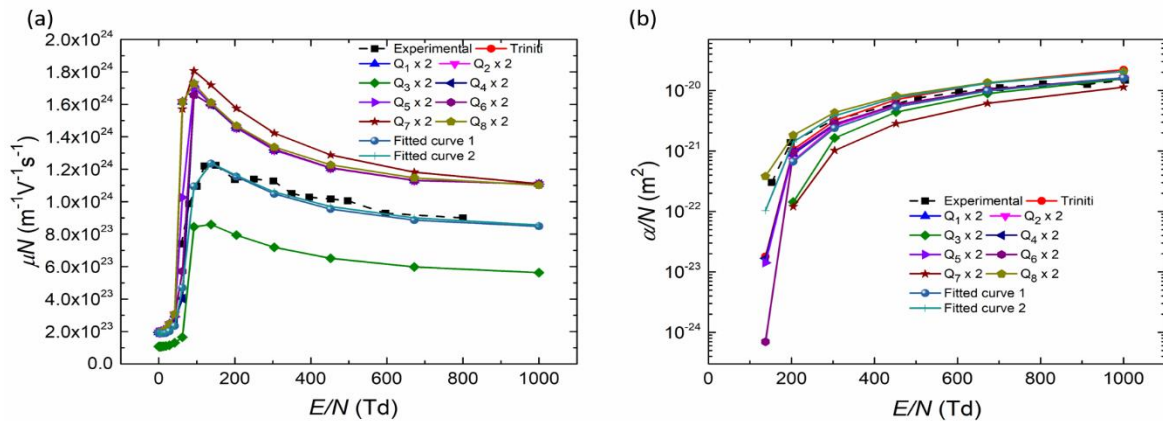
Figure 17: Calculated reduced mobility (a) and Townsend coefficient (b), by multiplying the various cross sections with a factor 2.

The first reactions to be tested are the attachments (Q_1 and Q_2). By multiplying them by a factor of 2, the reduced mobility does not present significant changes. On the other hand, when the effective cross sections (Q_3) are multiplied by 2, this leads to a decrease in reduced mobility. Similarly, to the previous case, we can observe some change in reduced mobility for Q_4, as a result of the multiplication factor. More specifically, the maximum in figure 17a drops and becomes narrower and it shifts to the right. When multiplying the cross section of vibrational excitation Q_5 with factor 2, the hill is shifted to the right, while for the vibrational stretching Q_6 the reduced mobility becomes lower and the maximum will move to the right. For the dissociation by excitation, Q_7, the reduced mobility will become higher (for the whole curve). Finally, if the ionization cross section Q_8 is multiplied by 2, only the values beyond the maximum will become higher. In general, we can say that the multiplication of the effective, rotational and vibrational cross sections by a factor of 2 will decrease the reduced mobility. On the other hand, doing the same for the rotational, bending and vibrational cross sections, we observe a shift of the maximum to the right. Finally, if we multiply the dissociation cross section by a factor 2, we see an increase of the reduced mobility.

For the Townsend coefficient, increasing the attachment cross section results in a lower Townsend coefficient, since the number of free electrons will decrease. By increasing the effective cross sections, the Townsend coefficient becomes even lower. By changing the rotational, bending and vibrational stretch cross sections, the Townsend coefficient will become lower as well. The Townsend coefficient with higher dissociative cross section will become also lower. By increasing the ionization cross section, the Townsend coefficient will become higher (due to the creation of more electrons). In general, we can conclude that by increasing the cross sections, with the exception of ionization (due to the increase in electrons), the Townsend coefficient will become lower.

Based on this knowledge, a set can be finally created that will be in close agreement with the experimental values. By changing the cross sections, it has to be taken into account that both the reduced mobility and Townsend coefficient will be influenced, except for the attachment reactions. In the end, two fitted sets were created. In the first one, the effective cross section Q_3 was multiplied by a factor 1.3, while the rotational cross section Q_4 was multiplied by a factor 1.2 (within the uncertainties typically associated with available cross sections). In the second set, we made the same changes, but in addition, we also multiplied the ionization cross section Q_8 by a factor 2. The fitted sets are pure illustrative and are an example of the non-uniqueness of the cross sections. They will therefore not be used in following tests.

4. Brief overview of Other Data

To further optimize the cross section set of Triniti, a literature study was performed to find additional information about which cross sections are the most important to include and to obtain an overview about the important data sets available.

In the beginning, two main review articles were consulted: Itikawa et al.[43] and Ness et al.[65] Both provide a dataset created either from the reviewed or calculated cross sections. From here, some articles involving datasets[66–68], while others related to specific processes, namely momentum transfer[69], rotations[43,64,70–74] and vibrational excitation[63,75] were found.

Over a range of reduced electric fields from 0 Td to above 90 Td, different cross sections have different importance to this work. At low fields (< 35 Td) the rotational cross sections have the biggest contribution, for intermediate ranges (35 – 90 Td) vibrational cross sections are more important, and in the higher fields range (> 90 Td) ionization and dissociative attachment are essential.

For polar molecules, rotational excitation is the dominant process in low energy collisions. Moreover, at energies below the vibrational threshold, the only inelastic process is rotational excitation, thus the rotational transition plays a significant role in slowing down electrons in a molecular gas.[43] The rotational process where $\Delta J = 1$ is the most efficient process.[70] Water, in general, will exhibit large rotational total cross sections, since it is a polar molecule and will therefore interact strongly with low energy electrons. However, obtaining rotational cross sections experimentally can be troublesome. This happens because the rotational levels of water lie very close together and electron beam experiments do not have enough resolution to resolve each rotational state.[43] In addition, swarm experiments can give very accurate cross sections for the sum of all overlapping reactions, but only estimates of partial cross sections can be obtained.[71] If partial cross sections come into play, the use of computational methods will be a big help. Itikawa et al. used the Born approximation to derive a formula to calculate the rotational cross sections[74] that is quite in use by many authors, like Ness et al,[65] who included around 100 calculated cross sections in their set.[65] However, more often the cross sections up to J = 3 are included.[68,72] Sometimes, the rotational cross sections are incorporated into the elastic cross sections, creating therefore "quasi-elastic" cross sections. This delivers results that do not match with the experimental data. It is thus important to have separate rotational and elastic cross sections.[65]

The biggest drawback from the papers mentioned above is that quasi none of them provide data (except some graphs). Therefore, we decided to keep on working with the LXCat database. However, the literature study has provided more insight into the importance of the cross sections. The most important insights are the recommendation to use elastic cross sections over effective cross sections[65] and the highlighted importance of the rotational cross sections.[65,70,76] An overview of the consulted papers can be found in Appendix A6.

5. Improving the Dataset

Considering the remarks of the last section, the Triniti set was further optimized using the LXCat database. For each reaction, the different cross sections were compared with the experimental data. Since more than 26 sets were created, only the most important ones will be discussed here. The results for reduced mobility will be discussed first. The first step considered was replacing the Triniti values that showed a small range, with cross sections that show a larger range of availability. As a result, set 1 was created, where Q_5 is replaced by data from the Hayashi database and Q_6 and Q_7 by data of the Morgan database. This gives us a set that is already closer to the experimental data (see figure 18a). The next step is to replace the effective cross sections by elastic cross sections. For this purpose, set 2 and 3 were created, where the values are replaced with data from Itikawa and Morgan, respectively. Set 2 has the maximum on the correct height but the maximum is too much on the left side and the values in the lower regime (before 50 Td) are too high. Set 3 provides a curve in agreement with the experimental data, but the absolute values are too low. Consequently, the rotations were replaced by the ones from the Itikawa set, because the Triniti set only includes one single cross section for all the rotations, which is also quite different from the ones found in other papers.[64,72,74] The problem here is that by adding the separate cross sections, the populations of the levels are needed, which cannot be easily included in Bolsig+. As a result of this, the results are too low. However, by removing the cross section of J(0 → 1) from the set (this decision was made after testing each of the cross sections separately), better results can be obtained. Important to mention is that this adjustment is only applied to be able to be run with Bolsig+, but later on, in the final set, all the Itikawa cross sections up to J = 3 will be run with the LoKI code. Set 1 and 2 served as basis for set 4 and 5, with each different rotation sets. Both curves obtained show a shape in good agreement with the experimental data, but they are too high and too low, respectively.

For all the sets, the Townsend coefficient is still too high (figure 18b). In further tests, more attachments, ionizations and excitations were added, but this did not provide any better results, for both reduced mobility and Townsend coefficient.

Since adding the elastic and rotational cross sections from the database is not sufficient and since they are quite important, more time should be spent on finding good cross sections for these processes.
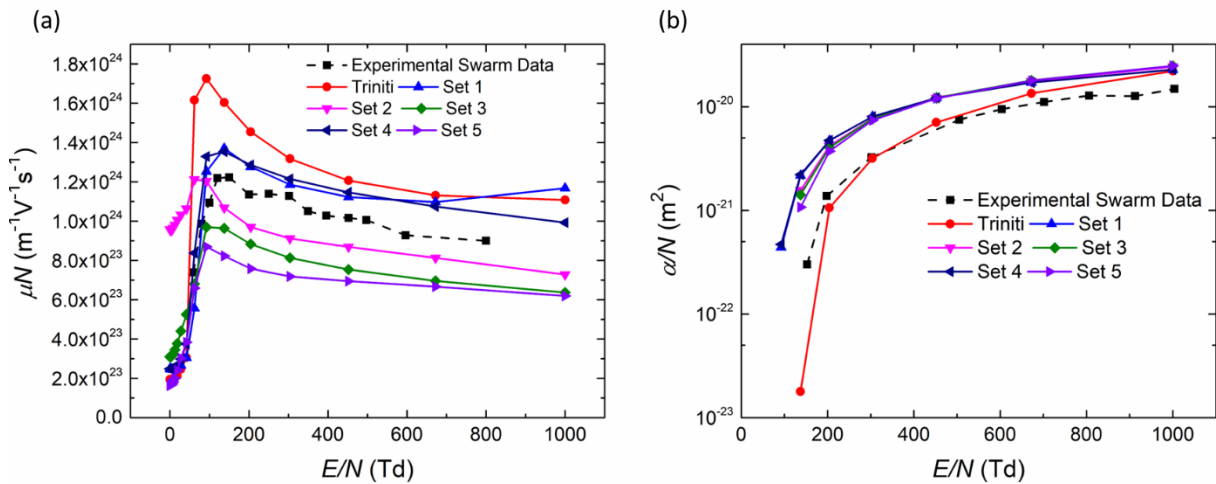
Figure 18: Calculated reduced mobility (a) and Townsend coefficient (b), obtained with new sets 1-5 (see text), compared to the experimental swarm data and the calculations with the original Triniti set.

6. Finding Elastic Cross Sections

As a next step we tried to obtain the elastic cross sections from the Triniti results (i.e. effective cross sections). This can be done since it is known that elastic CS = effective CS – inelastic CS. The inelastic cross sections are all the cross sections from the set, not including the effective one. Since all the cross sections have different points where data is given, the inelastic cross sections were interpolated, so they could be deduced from the effective ones. However, the obtained cross sections show negative results. This is a sign that the effective cross sections are not reliable. To correct the obtained elastic cross sections, they will be compared with the ones from Itikawa and Hayashi.
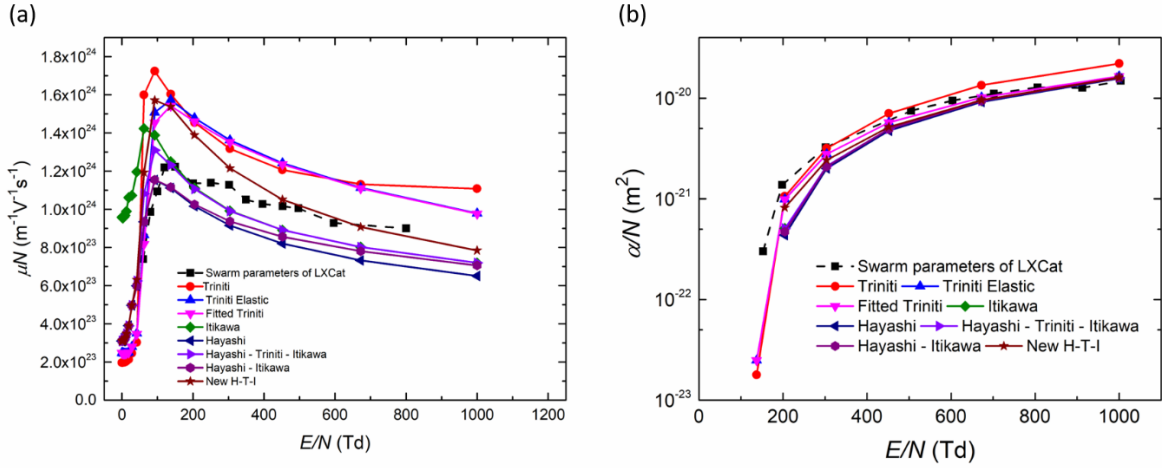
Figure 19: Influence of the different sets of elastic cross sections on the reduced mobility (a) and the Townsend coefficient (b).

The negative values were first changed to be zero. Next, they were fitted to the values comparable with Itikawa and Hayashi. Later on, sets were created that are a mix of the different elastic cross sections. Each time the reduced mobility and Townsend coefficient was calculated. The sets with the better results were selected and can be seen in figure 19a and 19b. None of the sets created overlaps with the experimental reduced mobility data, but some come close. Every curve created is better than the original one from Triniti. The elastic cross sections obtained from the Triniti set are also already better. However, it can be stated that the combination of Hayashi, Triniti and Itikawa corresponds most to the experimental curve. For the Townsend coefficient, every curve showed a better match with the experimental data, with the optimized elastic cross sections from Triniti giving the best overlap.

7. Optimizing Rotational Cross Sections

Since the rotational cross sections provided by Triniti show discrepancies, a new rotational cross section set had to be obtained. It should be mentioned that due to the different sets of rotational levels in water, it is assumed that:

$$Q(0 \rightarrow J) = \sum_\tau Q(0_0 \rightarrow J_\tau) \tag{AR1}$$

The rotational set from Itikawa is discussed extensively in the literature, nevertheless by using it in Bolsig+, it does not give good results due to the lack of populations. Due to small interlevel spacing, water molecules in the gas phase at finite temperature will be populated over a large range of rotational states.[43] The separate rotations from Itikawa will, however, be used to create a new set.
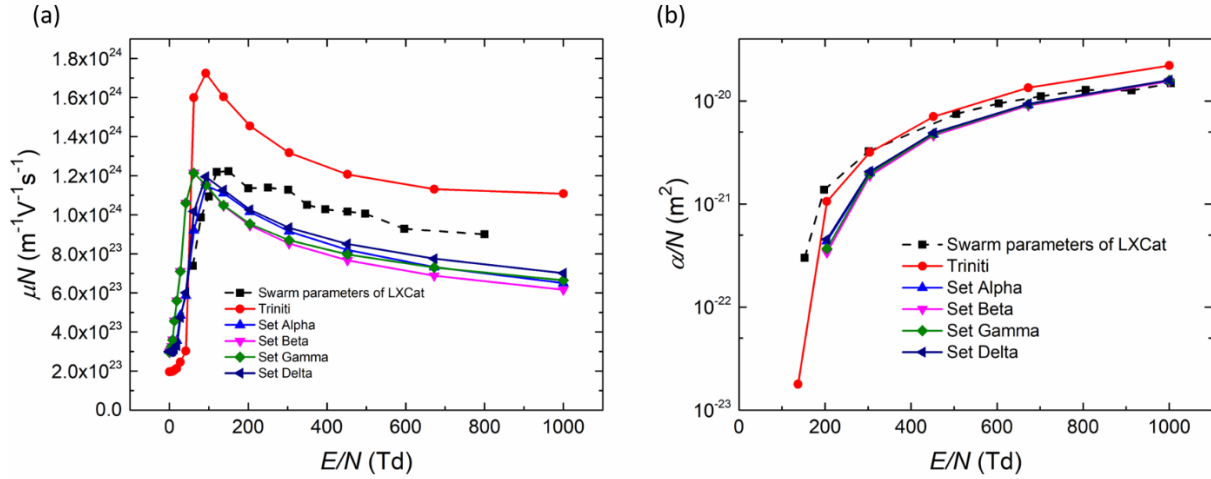
Figure 20: The sets with optimized rotational cross sections: set alpha contains Hayashi Elastics and the longer rotational cross sections of Triniti; set Beta contains Hayashi and rotations for J = 2 and J =3, set Gamma contains Hayashi and Itikawa elastics a own made set 3, set Delta contains HI-elastics and rotations for J = 2 and J =3; reduced mobility (a) and Townsend coefficient (b)

The approach here was to firstly try to optimize the rotational cross sections from Triniti, just to see what they would give. This was done by elongating the range of the cross sections where possible and increasing the value. Moreover, sets were created containing the summed cross sections of Itikawa. Additionally, sets were formed containing mixtures of separate cross sections. This means that the beginning of the set contained Q(0 → x) and then continued to Q(0 → y) etc. Again, not all sets will be showed, but only the best results. The reduced mobility for all sets shown demonstrates already a better fit than without the optimized rotations. There is still room for improvement for the Townsend coefficient, but for higher levels the overlap is already quite good.

8. Choosing the Best Set

After testing more than 75 sets, two sets, called A and C, were constructed using the background information obtained by trial and error applied in previous sections. Set A shows better overlap for the reduced mobility, while set C shows very good agreement with the Townsend coefficient. However, the reduced mobility calculated with set C is not very good, and therefore set A was chosen. The Boltzmann solver from IST, LoKI, was used to calculate the resulting swarm parameters and therefore, the sets with the rotations of Itikawa were used as well. Additionally, to create a more extensive and complete set, adding more attachments, ionizations and excitations was tried. However, this did not deliver better results.

The final set A contains the following cross sections. They are plotted in figure 22 as a function of electron energy:

Reaction		Source
Q_1 *Dissociative Attachment*	$e + H_2O \rightarrow H_2 + O^-$	Triniti[62]
Q_2 *Dissociative Attachment*	$e + H_2O \rightarrow OH + H^-$	Triniti[62]
Q_3 *Elastic*	$e + H_2O \rightarrow e + H_2O$	Hayashi[77,78]
Q_4 *Excitation*	$e + H_2O \rightarrow e + H_2O_{rot}$	New Rot 3/Own Set
Q_5 *Excitation*	$e + H_2O \rightarrow e + H_2O(010)$	Itikawa[43]
Q_6 *Excitation*	$e + H_2O \rightarrow e + H_2O(100,001)$	Triniti[62]
Q_7 *Dissociation*	$e + H_2O \rightarrow e + H + OH$	Triniti[62]
Q_8 *Ionization*	$e + H_2O \rightarrow e + e + H_2O^+$	Triniti[62]
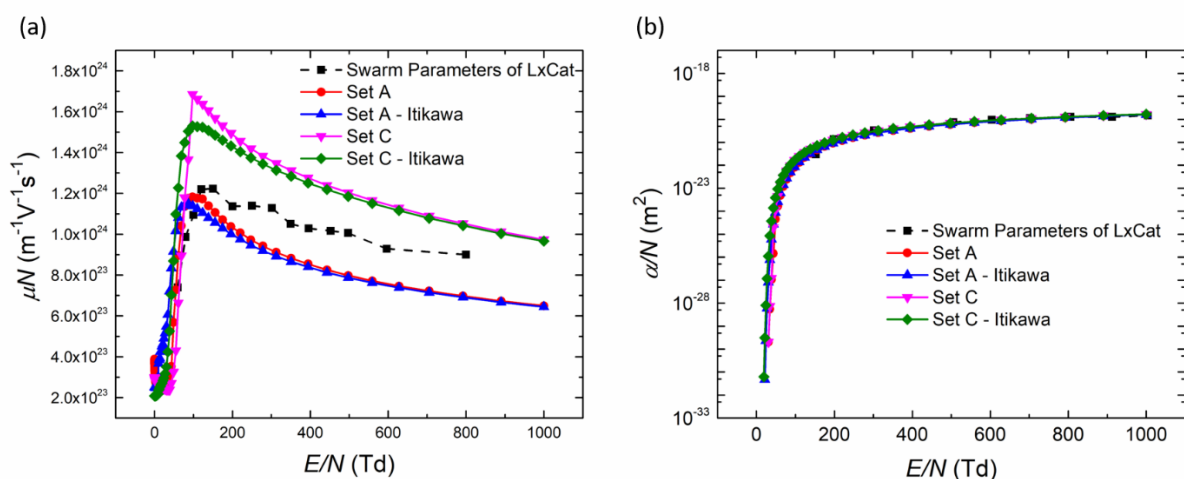
Figure 21: Results obtained using the LoKI code from set A and C one time with the new rot 3 set, and one time with the use of Itikawa's rotation: reduced mobility (a) Townsend coefficient (b)
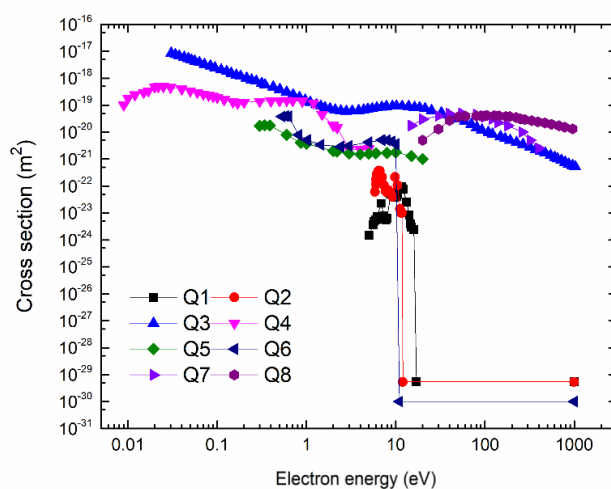
Figure 22: Best cross section set A as a function of electron energy.

9. Continuation of the Work

Due to the limited time of this master thesis, we had to stop here; therefore, the sets are not optimal yet, but are the best that could be obtained within this time frame. The obtained set A can be still optimized by using techniques to directly obtain the cross sections from the graphs out of the above-mentioned papers[43,63–75] and include them in the tests. Furthermore, using Itikawa's approximation,[74] cross sections for higher J-values can be obtained. As already mentioned before, this is also an important part due to the small rotational interlevel spacing. The only drawback again is that another Boltzmann solver, that is able to include the populations, like LoKI, has to be used.

10. EEDF

From the obtained cross sections, the EEDF can be calculated. This is shown here for a gas temperature of 300 K, a reduced electric field of 100 Td, a mixture of CO_2/H_2O that will be used in the kinetic models (see Part 2). The cross sections for CO_2 are obtained from the IST database in LXCat.[46] The results are plotted in figure 23, for different H_2O concentrations, ranging from 0 to 100%.

The H_2O-curve up to 1 eV shows a sharp decrease in electron energy, which can be also found in the curves of the mixtures, albeit somewhat less pronounced. The more H_2O, the more the curve will decrease. This can be accounted to the rotational excitations, that are very important in the H_2O cross sections set. Due to these rotational transitions, water will slow down the electrons, and thus their energy will be lower.[43] Between 1 eV and 5 eV, the cross sections are higher in case of the higher CO_2-fractions. The decrease in values will slow down for pure H_2O, due to less rotational excitation. This range (1 – 5 eV) is most important for vibrational excitations of H_2O. After ~5 eV a sharp decrease in the EEDF can be seen. This is due to the fact that more energetic processes, like ionisations, attachments and dissociations, will occur and therefore take up the energy. In addition, it can be noticed that in pure H_2O the EEDF is again slightly higher than in pure CO_2 in this energy range. The graph containing the CO_2-cross sections can be found in Appendix A7.
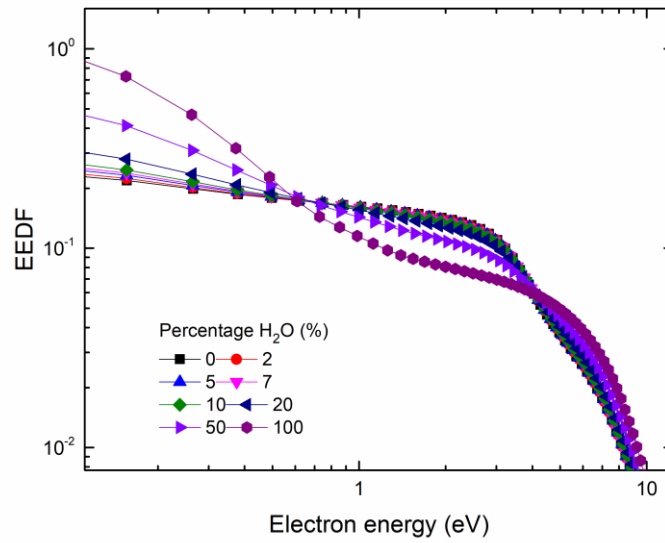
Figure 23: EEDF calculated from set A for the electron collisions with H_2O, and from the IST-set[46] for the electron collisions with CO_2, using different concentrations of water

11. Dissociation and Ionization Rate coefficients

Dissociation Rate Coefficients
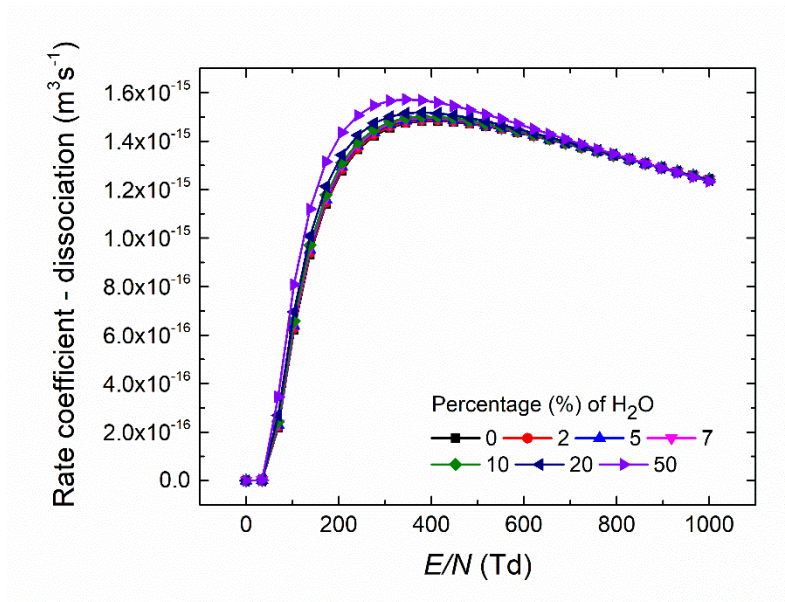
Figure 24 Dissociation rate coefficient for CO_2, obtained through Bolsig+ calculations.

To better understand the influence of the changed EEDF on the actual reactions, the dissociation and ionization rate coefficients of the mixture will be plotted. Figure 24 shows the dissociation rate coefficient of CO_2. Here a gradual increase can be seen with an increasing H_2O percentage. This indicates that by adding more H_2O, we obtain more electron impact dissociation per CO_2-

molecule. This can be due the higher electron energy above 5 eV for mixtures with H_2O, as can be seen in the EEDF.

Ionization Rate Coefficients

Figure 25a and Appendix A8 show the ionization rate coefficients of CO_2 and H_2O, respectively, for different percentages of H_2O. A similar trend can be found here: a higher H_2O fraction stimulates a rise in the ionization coefficient. Additionally, the higher the electric field, the more pronounced is the effect. This indicates that a mixture stimulates the ionization for both CO_2 and H_2O. Moreover, the ionization coefficient of H_2O is higher than the ionization coefficient of CO_2, due to the slightly higher ionization cross section. Interesting to notice is that the ionization energy of H_2O and CO_2 is 12.6 eV and 13.8 eV, respectively, and thus it only differs ~1.2 eV. The EEDF also shows overlap in the ionization area (between 10-15 eV).
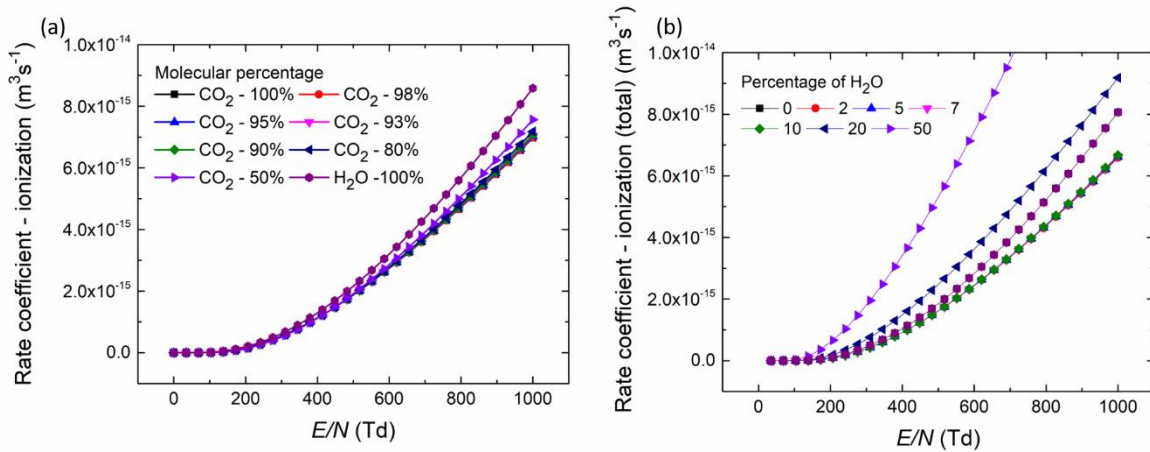
Figure 25 Ionization rate coefficients: individual ionization rate coefficient for H_2O and CO_2 (a); total ionization coefficient. Both increase for higher fractions of H_2O (b).

Figure 25b shows a similar trend for the total ionization coefficient (fraction CO_2·ionization rate coefficient CO_2 + fraction H_2O · ionization rate coefficient H_2O). Direct ionization (as it is the case here, indicating also that there is no direct dissociation) occurs when the electrons do not exceed too much the ionization potential. Since here an increase in the ionization rate coefficients is noticed, one can say that more electrons with the right energy will occur in the mixture. This will be due to the fact that the ionization coefficients of pure H_2O are higher, since it has higher cross sections, resulting in more total ionization in mixtures with CO_2 compared to pure CO_2. Since the electrons play an important role in sustaining the plasma, the electron impact reactions (and their changes) will as well have an influence on the outcome of the simulations.

B. Part 2: The Kinetic Model

1. Rate coefficients of V-T Relaxation of the CO_2 Vibrational Levels by CO_2 and H_2O

The results obtained from the calculation of Theory and Methods C.5 are shown in figure 26. The rate coefficients of the CO_2-H_2O V-T relaxation collisions are compared with those of the CO_2-CO_2 V-T relaxations calculated using the Kozak and Bogaerts[1] data. The rate coefficients of CO_2(001)-quenching are obtained from Blauer.[59] For $v_3 > 1$, the rate coefficients are scaled according to the SSH-theory, explained in part Theory and Methods C.5. As can be seen in the figure, the CO_2-H_2O collisions have overall higher reaction coefficients, even by several orders of magnitude. This indicates that water will quench the CO_2 asymmetric vibrational mode levels more than CO_2. Therefore, we expect that the inclusion of water will show a lower population of the CO_2 vibrational levels.
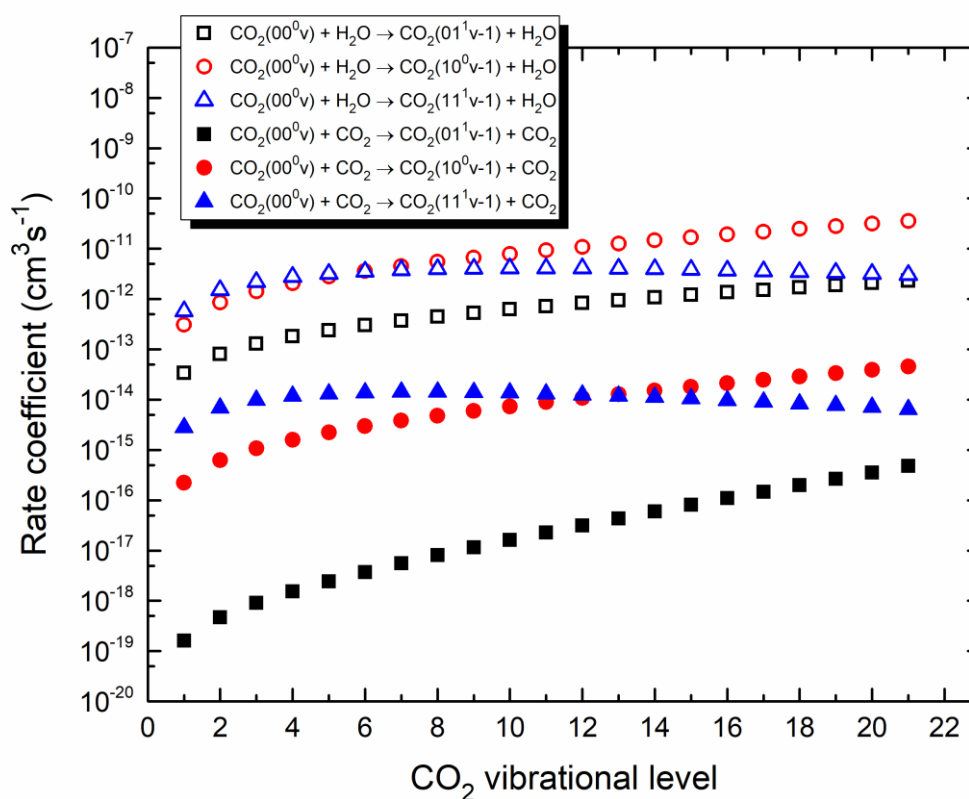
Figure 26 Scaled rate coefficients of the quenching of the asymmetric vibrational levels by CO_2 and H_2O. It can be observed that the H_2O rate coefficients are higher than the ones for CO_2.

2. Results of the model of Kozak and Bogaerts

As a first step in a more extensive research into the influence of H_2O on the CO_2 chemistry, the effect of the addition of V-T reactions into the set will be tested. By using this step-by-step approach, insight can be gained in the influence of the different reactions on the total chemistry set. Although the results can give a deeper understanding of the processes, it should be kept in mind that they are not yet a representation of reality. This is due to the lack of other reactions, including V-V-relaxation and chemical processes. Consequently, the results are an intermediate step into obtaining final results. An important note to make here is that due to the fact that no extra reactions including water chemistry were added, it was decided to remove V-T relaxation of H_2O vibrational levels upon collision with either H_2O or CO_2 molecules, since they have no added value in this stage of the research.
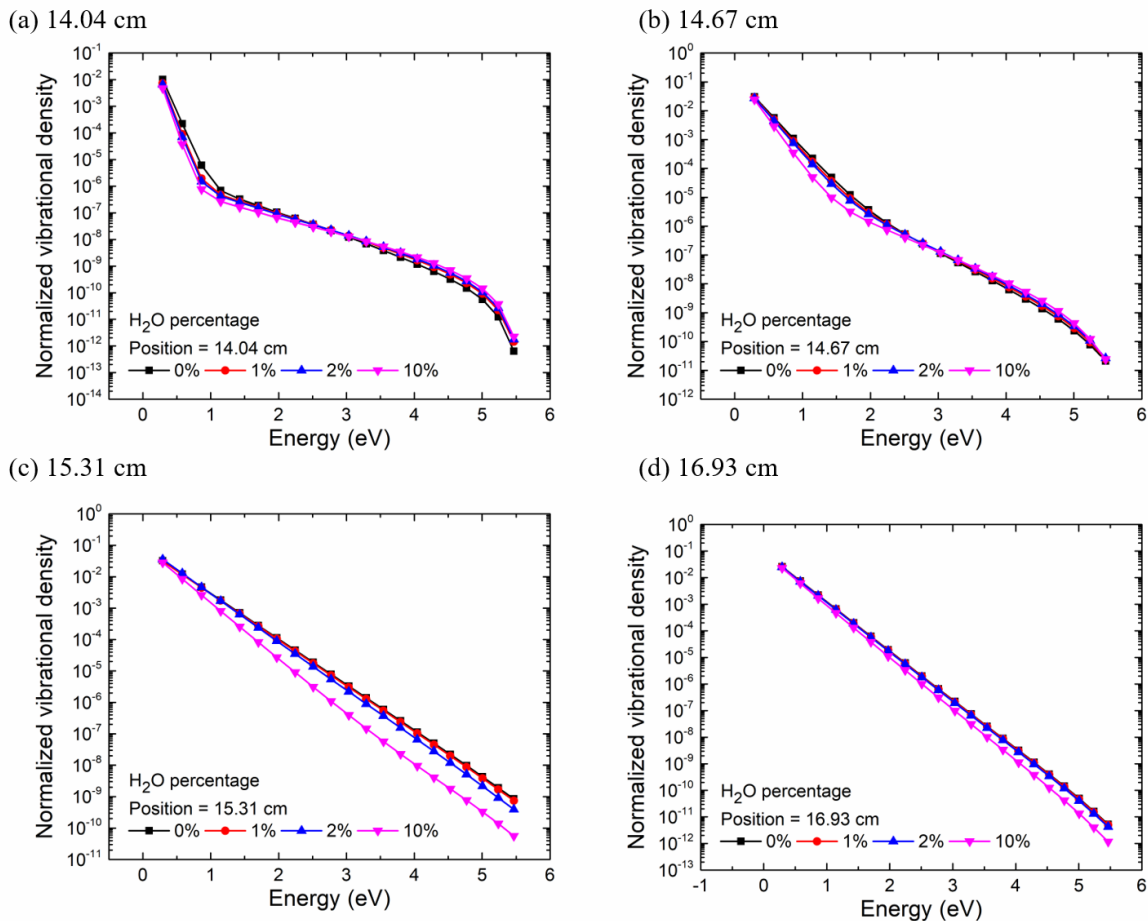
Figure 27: VDFs calculated with the Kozak and Bogaerts model, for pure CO_2 and 1, 2 and 10% of H_2O addition, at different positions in the plasma tube (see text) – beginning of the plasma at 14.04 cm (a), middle of the plasma at 14.67 cm (b), middle of the plasma at 15.31 cm (c), just outside the plasma at 16.93 (d). The x-axis represents the asymmetric vibrational levels, therefore the ground level is not added

Figure 27 (a, b, c and d) shows the VDFs, calculated with the Kozak and Bogaerts model, for 0%, 1%, 2% and 10% of water, for different positions along the discharge tube (figure 12). Note that the plasma runs from ~13.5 cm to ~16.5 cm. It can be noticed that most VDFs are thermalized (i.e. they show a Boltzmann distribution) after ~15 cm (which is still in the plasma). For the positions 14.04 cm and 14.67 cm, it can be noticed at first that the lower vibrational levels (up to $v_3 = 9$, which corresponds to an energy of 2.51 eV) are slightly quenched in the plasma upon H_2O addition (see figure 27(a, b)). However, the higher populated levels show a slight increase in population. This effect disappears further along the tube, and thus further in the plasma. Additionally, thermalized curves are obtained. These results partially correspond to our expectations, since water is predicted to quench the levels, but a greater effect was expected. In addition, the increase in densities of the higher vibrational levels were not expected.

Although the limited number of papers on CO_2/H_2O-mixtures available show mostly a strong quenching reaction[12,34], Chen et al.[79] reported a higher CO_2 conversion in their experiments, which can help us understand the results. A possible explanation is a cooling effect caused by H_2O addition. Indeed, a drop in average gas temperature in the plasma region was calculated in our model, from 2269 K for pure CO_2 to 1976 K for 10% H_2O. Higher temperatures reduce the population of CO_2 vibrational levels (due to the increase of the V-T reaction rate coefficients),[79] and therefore in this case a cooling effect has a positive outcome. At the same time, an increase in the average electron temperature with an increasing concentration of H_2O (from ~0.94 eV for pure CO_2 to ~1.80 eV for 10% H_2O) was predicted by the model, which in this case is beneficial for the higher vibrational excitation of CO_2.[79] Indeed, as can be seen in figure 28, it leads to an increase in the fraction of energy transferred to the higher asymmetric vibrational mode levels, but a decrease in energy transferred to the lower vibrational levels. Therefore, an increase in electron temperature is not beneficial for the electron energy transfer to lower vibrational energy levels. The fact that the higher vibrational levels are depopulated again further along the tube upon H_2O addition (see figure 27(c, d) can be attributed to the lower T_e, and faster decrease in electron temperature compared to the gas temperature. Moreover, the rate coefficients for quenching are dependent on the gas temperature, which increases more slowly than the electron temperature and will therefore need more time to become a more important mechanism, explaining the increased population of the higher vibrational levels in the beginning of the plasma. Towards the end of the plasma, thermalisation can be observed, which results in lower electron temperature, and thus the quenching becomes more dominant. When

the gas leaves the plasma, again the electron temperature will drop faster than the gas temperature, which makes the quenching process more prominent.

Additionally, the increased concentration of H_2O creates changes in the EEDF. The different energy distribution can also (partially) account for the intensification of the results mentioned above. Note that, due to the complexity of plasmas, more factors can come into play, that might be overlooked at this time. On the other hand, due to the small changes that occur (as seen mostly in 1% and 2% of H_2O), the results might also depend on uncertainties of the calculations. In general, it can be suggested that, when the quenching becomes the dominant process, further in the plasma, the expected quenching occurs.

The hypotheses stated above, i.e., influence of the gas and electron temperature, and electron energy distribution (calculated with inclusion of the newly provided cross sections of H_2O), can be tested by (i) running simulations with a constant temperature (gas and/or electron), and (ii) removing the electron impact reactions of water from the model. However, due to the limited amount of time available, these hypotheses could not be tested before completion of the thesis. It should also be noted that these results are the first ones obtained through the usage of the customized code. Therefore, there is no knowledge yet on the uncertainties of this particular code. Additionally, even though the code was checked multiple times, there always exists a chance that some mistakes stayed unnoticed. In Appendix A9, the VDF for all the positions of the different concentrations can be found.
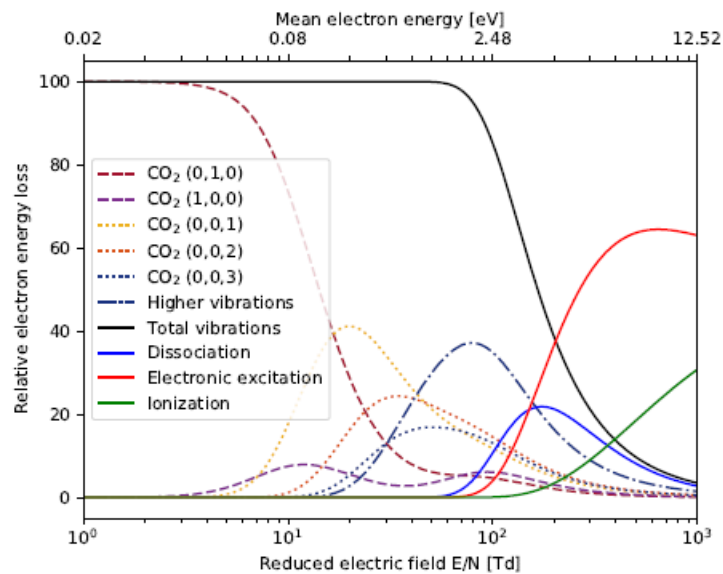
Figure 28: Fractions of non-thermal CO_2-discharge energy transferred from plasma electrons to different channels of excitation. It can be noticed that for (asymmetric) higher vibrations, the maximum of the curves moves to the right. Therefore, more energy will be transferred to higher levels when the electron temperature increases as it is the case here. Note that this is for pure CO_2, however due to the small fractions included, it is assumed that this will not change drastically.[80]

Finally, it is important to note that the results presented are preliminary. During the runs some problems were observed with the electron temperature, which is an artefact of the base code. To temporally solve this problem, the dissociative attachment process of CO_2 was removed.

3. Results of the model of Silva et al.

The same step-by-step approach as for the Kozak and Bogaerts model[1] was taken. Note that for this model no electron impact reactions for water were added. Another important remark that has to be made is that the model of Kozak and Bogaerts[1] describes a MW plasma, while the code of Silva et al.[2] applies to the relaxation of a pulsed DC glow discharge. Additionally, this model only accounts for the lower lying CO_2 levels.
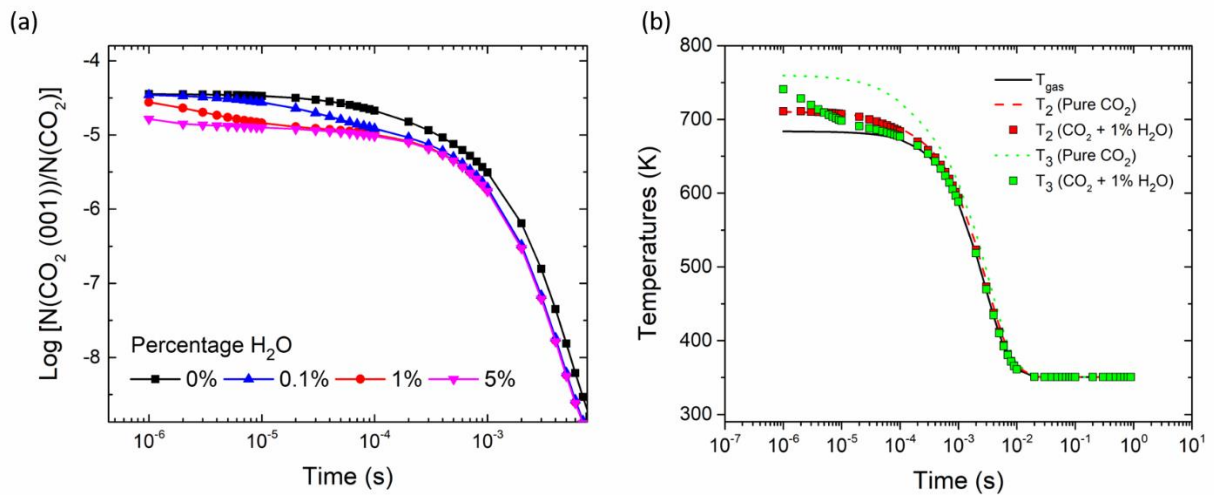
Figure 29 Results of the Silva et al. model: time-evolution of the densities of vibrationally excited $CO_2(001)$ (a); vibrational temperature for 1% of water (b)

Figure 29a shows the evolution of the vibrationally excited $CO_2(001)$ levels. We can observe that increasing the concentration of H_2O leads to the strong quenching of vibrationally excited CO_2. This is also reflected in the evolution of the vibrational temperature (figure 29b) related to the asymmetric mode of vibration, i.e. T_3. Note that a decrease of roughly 70 K is observed due to inclusion of 1% of H_2O. These results match with the expectations mentioned in subchapter 3A.1 that increasing the concentration of H_2O leads to a stronger quenching of vibrationally excited CO_2 This comes from the following reactions included in the model of Silva et al[2]:

$$CO_2(00v) + H_2O \leftrightarrow CO_2(01v\text{-}1) + H_2O, \qquad (51)$$

$$CO_2(00v) + H_2O \leftrightarrow CO_2(10v\text{-}1) + H_2O, \qquad (52)$$

$$CO_2(00v) + H_2O \leftrightarrow CO_2(11v\text{-}1) + H_2O, \qquad (53)$$
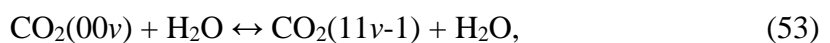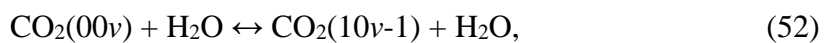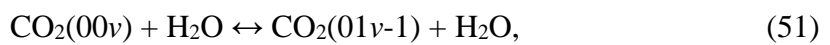
in which the asymmetric states are quenched in collisions with H_2O molecules. As expected, the quenching of CO_2 bending states is less effective, for the H_2O concentrations tested, as shown in figure 29b. Indeed, we can see that T_2 remains almost unchanged as a result of the inclusion of H_2O. Figures containing more concentrations can be found in Appendix A10.

These results are slightly different from the ones obtained from the model of Kozak and Bogaerts.[1] There can be different reasons for this: (i) the difference in the plasma discharge used, because as it was mentioned in the state of the art, MW plasma is known for stimulating the vibrational excitation channel, (ii) the calculation of the vibrational temperature in the off-mode of the pulse, and therefore there is no fast increase of electron temperature, as was mentioned above as a possible explanations, (iii) the inclusion of only lower lying levels, while the model of Kozak and Bogaerts does not include all the lower lying levels, and therefore reaction 41 was included instead of the separate reactions 51-53, (iv) differences in the rate coefficients for V-T and V-V transfers in pure CO_2 (due to the usage of different scaling models), and (v) the lack of electron impact reactions with H_2O – since this is one of the hypotheses stated and it influences the EEDF, which again has an influence on the different processes. However, there are too many other variables and differences between the codes that need to be taken into account before an overall conclusion can be made. In general, it can however be stated from this model that the lower lying levels in a glow discharge are quenched by H_2O.

Chapter 4: Conclusion

A. Conclusion

A kinetic modelling study was performed to obtain more insight in the vibrational kinetics of an CO_2/H_2O-mixture. As a first step, a cross sections set for H_2O electron impact reactions was created, using a swarm-based method and an extensive literature study. This resulted in a cross section set containing 8 reactions, i.e., (i) two dissociative attachment cross sections, (ii) one elastic momentum transfer cross section, (iii) four vibrational cross sections, and (iv) one ionization cross section. From this set, the EEDF was calculated. Adding water introduced changes into the EEDF, most pronounced in the lower energy range (< 1 eV), where the rotational cross sections play an important role in slowing down the electrons. Additionally, higher dissociation rate coefficients and total ionization rate coefficients were observed with an increasing fraction of water.

Secondly, the model of Kozak and Bogaerts[1] was used to calculate the normalised vibrational densities of the CO_2 asymmetric vibrational levels. This was done for pure CO_2, 1%, 2% and 10% of water. The results showed an overall decrease in densities of the higher asymmetric vibrational levels, which was expected. However, the decrease was not as prominent as expected. Additionally, a small increase in vibrational densities of the higher vibrational levels ($v_3 > 10$) was noticed in the beginning of the plasma. Different hypotheses can be made to account for these results, (i) a lower gas temperature and (ii) a higher electron temperature, favour the (higher) vibrational population, and (iii) changes in the EEDF due to addition of cross sections for water. Nevertheless, it should be noted that the results are preliminary due to some problems with the electron temperature in the code, that will first have to be solved.

Finally, the model of Silva et al.[2] shows the quenching of the lower asymmetric vibrational levels, but not for the other vibrational modes, as was initially expected. This difference in results with the model of Kozak and Bogaerts can be explained by (i) the difference in plasma discharge, (ii) calculations in the afterglow (iii) the difference in the vibrational levels included in the model, (iv) difference in the rate coefficients used for pure CO_2, and (v) lack of the H_2O electron impact reactions in this model. In general, it can be concluded, that the CO_2/H_2O-mixture shows a complicated behaviour that gives very interesting results. However, more research is needed to clarify the results and to gain more insight.

B. Prospects

As mentioned throughout the whole Results and Discussion chapter, this research is a first attempt to gain more insight into the complex behaviour of the CO_2/H_2O-mixture. Due to the limited time of a master thesis, only the first steps could be taken. Thus, the work does not end here. A first step that must be taken is the further optimization of the H_2O-cross section set, which includes further exploration of the available cross sections sets and eventual expansion of it with more reactions. Secondly, it would be necessary to test more concentrations of water, definitely in the Kozak and Bogaerts model, to see if the increase in populations of higher vibrational levels (for positions below 15 cm in the plasma), continues. Thirdly, the influence of pressure, initial gas temperature, SEI, input power and reactor geometry should be tested. This might provide important insights and maybe even indications for an optimal set-up. Next, to check the hypotheses, some simulations with a constant temperature (gas and/or electron) and without electron impact reactions from water should be performed. Finally, to continue this research, more reactions should be added to the set, to make the models more complete, including V-V-reactions and chemical reactions. Only when the model is more complete, the effect of the fraction H_2O, pressure, temperature, etc. can be thoroughly evaluated.

C. Acknowledgments

First of all, I would like to thank professor Annemie Bogaerts and professor Vasco Guerra very much for the amazing opportunity to enjoy an Erasmus in the beautiful country of Portugal and the endless support I was lucky to receive. Thank you very much for the countless hours of meetings, discussions and help provided.

Thank you, professor Guerra for the amazing reception in the research group, that made feel instantly at home and guiding me through my first steps in the world of CO_2-conversion. I will never forget the important lessons learned about research and science from you that will have a lasting impact on my future career.

Thank you, professor Bogaerts for teaching me my first lessons about plasmas that sparked my interest instantly in my early bachelor years and that would shape my future path. Thank you for all the chances and guidance given to me over the years and being, during my time abroad, a point at home where I could always fall back on.

A special thanks to my mentor and friend dr. Tiago Silva for being the first one to receive me and making my first day already unforgettable. I will never forget the endless hours spend working together in the office and all the great advice and help I was lucky to receive. I am deeply indebted to you and I would never have gotten this far without you.

I would also like to thank Stijn Heijkers and Vincent Vermeiren for the help with the code and long discussions about it.

As last, but not least, a big thank you to my family and friends for all the support I received. In special I would like to thank my Alameda 41-family for all the countless times they had to listen to my complaints, sad and happy moments about this master thesis and supported me until the end.

Thank you all.

Bibliography

(1)   Kozàk, T.; Bogaerts, A. *Plasma Sources Sci. Technol.* **2014**, *23* (4).

(2)   Silva, T.; Grofulović, M.; Klarenaar, B. L. M.; Morillo-Candas, A. S.; Guaitella, O.; Engeln, R.; Pintassilgo, C. D.; Guerra, V. *Plasma Sources Sci. Technol.* **2018**, *27* (1), 015019.

(3)   Senguptan, S. *The New York Times*. March 29, 2018.

(4)   IPCC. *Climate Change 2013: The Fifth Assessment Report*; 2014; Vol. 5.

(5)   Weart, S. R. *The discovery of global warming': New histories of Science, Technology, and Medicine*, First.; Harvard University Press, 2003.

(6)   Arrhenius, S. *Philos. Mag. Ser. 5* **1896**, *41* (251), 237–276.

(7)   Callendar, G. S. *Q. J. R. Meteorol. Soc.* **1938**, *64* (1909), 223–240.

(8)   Keeling, C. D. *Tellus* **1960**, *12* (2), 200–203.

(9)   European Commission. *Energy 2020. A strategy for competitive, sustainable and secure energy*; 2010.

(10)   European Commision. *A policy framework for climate and energy in the period from 2020 to 2030*; 2014.

(11)   Goede, A. P. H. *EPJ Web Conf.* **2015**, *98*, 07002-1-07002-26.

(12)   Snoeckx, R.; Bogaerts, A. *Chem. Soc. Rev.* **2017**, *46*, 5805–5863.

(13)   Kozák, T.; Bogaerts, A. *Plasma Sources Sci. Technol.* **2014**, *24* (1), 015024.

(14)   Heijkers, S.; Snoeckx, R.; Kozák, T.; Silva, T.; Godfroid, T.; Britun, N.; Snyders, R.; Bogaerts, A. *J. Phys. Chem. C* **2015**, *119* (23), 12815–12828.

(15)   Snoeckx, R.; Heijkers, S.; Van Wesenbeeck, K.; Lenaerts, S.; Bogaerts, A. *Energy Environ. Sci.* **2016**, *9* (3), 999–1011.

(16)   Chen, G.; Silva, T.; Georgieva, V.; Godfroid, T.; Britun, N.; Snyders, R.; Delplancke-Ogletree, M. P. *Int. J. Hydrogen Energy* **2015**, *40* (9), 3789–3796.

(17)   Silva, T.; Britun, N.; Godfroid, T.; Snyders, R. *Plasma Sources Sci. Technol.* **2014**, *23* (2).

(18)   Fridman, A. *Plasma Chemistry*, 2nd ed.; Cambridge University Press: Drexel, 2008.

(19)   Rusanov, V. D.; Fridman, A. a.; Sholin, G. V. *Uspekhi Fiz. Nauk* **1981**, *134* (June), 185.

(20)   Asisov, R. I.; Vakar, A. K.; Jivotov, V. K.; Krotov, M. F.; Zinoviev, O. A.; Potapkin, B. V; Rusanov, A. A.; Rusanov, V. D.; Fridman, A. A. *Proc. USSR Acad. Sci.* **1982**, *271* (1).

(21)   Adamovich, I.; Baalrud, S.; Bogaerts, A.; Bruggeman, P. *J. Phys. D. Appl. Phys.* **2017**, *50*, 323001.

(22)   Spencer, L. F.; Gallimore, A. D. *Plasma Sources Sci. Technol.* **2013**, *22* (1).

(23)   Nunnally, T.; Gutsol, K.; Rabinovich, A.; Fridman, A.; Gutsol, A.; Kemoun, A. *J. Phys. D. Appl. Phys.* **2011**, *44* (27).

(24)   Aerts, R.; Somers, W.; Bogaerts, A. *ChemSusChem* **2015**, *8* (4), 702–716.

(25)   Wang, Q.; Yan, B. H.; Jin, Y.; Cheng, Y. *Plasma Chem. Plasma Process.* **2009**, *29* (3), 217–228.

(26)   Snoeckx, R.; Zeng, Y. X.; Tu, X.; Bogaerts, A. *RSC Adv.* **2015**, *5* (38), 29799–29808.

(27) Chung, W. C.; Pan, K. L.; Lee, H. M.; Chang, M. B. *Dry reforming of methane with dielectric barrier discharge and ferroelectric packed-bed reactors*; 2014; Vol. 28.

(28) Cho, W.; Ju, W. S.; Lee, H.; Baek, Y. S.; Kim, Y. C. *Proceedings of 7th International Conference on Carbon Dioxide Utilization*; 2004.

(29) Wu, A.; Yan, J.; Zhang, H.; Zhang, M.; Du, C.; Li, X. *Int. J. Hydrogen Energy* **2014**, *39*, 17656–17670.

(30) Chun, Y. N.; Yang, Y. C.; Yoshikawa, K. *Catal. Today* **2009**, *148* (3–4), 283–289.

(31) Maya, L. *J. Vac. Sci. Technol. A* **2000**, *18*, 285–287.

(32) De Bie, C.; van Dijk, J.; Bogaerts, A. *J. Phys. Chem. C* **2016**, *120* (44), 25210–25224.

(33) Savinov, S. Y.; Lee, H.; Song, H. K.; Na, B. K. *Korean J. Chem. Eng.* **2002**, *19* (4), 564–566.

(34) Snoeckx, R.; Ozkan, A.; Reniers, F.; Bogaerts, A. *ChemSusChem* **2017**, *10* (2), 409–424.

(35) Futamura, S.; Kabashima, H. *Synthesis Gas Production from CO2 and H2O with Nonthermal Plasma*; Elsevier Masson SAS, 2004; Vol. 153.

(36) Chen, G.; Godfroid, T.; Britun, N.; Georgieva, V.; Delplancke-Ogletree, M. P.; Snyders, R. *Appl. Catal. B Environ.* **2017**, *214*, 114–125.

(37) Neyts, E. C.; Yusupov, M.; Verlackt, C. C.; Bogaerts, A. *J. Phys. D. Appl. Phys.* **2014**, *47*, 29.

(38) Itikawa, Y. *J. Phys. Chem. Ref. Data* **2002**, *31* (3), 749–767.

(39) Atkins, P.; Paula, J. De. *Physical Chemistry: Thermodynamics, Structure, and Change*, Tenth.; W.H Freeman and Company, 2006.

(40) Herzberg, G. *Molecular Spectra and Molecular Structure II: Infrared and Raman of Polyatomic Molecules*, Seventh.; D. Van Nostrand Company INC.: Princeton, 1950.

(41) Suzuki, I. *J. Mol. Spectrosc.* **1968**, *25* (4), 479–500.

(42) Bogaerts, A.; Wang, W.; Berthelot, A.; Guerra, V. *Plasma Sources Sci. Technol.* **2016**, *25* (5), 055016.

(43) Itikawa, Y.; Mason, N. *J. Phys. Chem. Ref. Data* **2005**, *34* (1), 1–22.

(44) Tennyson, J.; Zobov, N. F.; Williamson, R.; Polyansky, O. L.; Bernath, P. F. *J. Phys. Chem. Ref. Data* **2001**, *30* (3), 735–831.

(45) Smith, D. F.; Overend, J. *Spectrochim. Acta Part A Mol. Spectrosc.* **1972**, *28* (3), 471–483.

(46) Grofulović, M.; Alves, L. L.; Guerra, V. *J. Phys. D. Appl. Phys.* **2016**, *49* (39).

(47) Petrović, Z. L.; Šuvakov, M.; Nikitović, Z.; Dujko, S.; Šaić, O.; Jovanović, J.; Malović, G.; Stojanović, V. *Plasma Sources Sci. Technol.* **2007**, *16* (1).

(48) Hasegawa, H.; Date, H.; Shimozuma, M. *J. Phys. D. Appl. Phys.* **2007**, *40* (8), 2495–2498.

(49) Petrović, Z. L.; Dujko, S.; Marić, D.; Malović, G.; Nikitović, Ž.; Šašić, O.; Jovanović, J.; Stojanović, V.; Radmilović-Radenović, M. *J. Phys. D. Appl. Phys.* **2009**, *42* (19).

(50) Inan, U. S.; Golkowski, M. *Principles of Plasma physics for Engineering and Scientists*; 2011.

(51) Hagelaar, G. J. M.; Pitchford, L. C. *Plasma Sources Sci. Technol.* **2005**, *14* (4), 722–733.

(52) Guerra, V.; Loureiro, J. *Plasma Sources Sci. Technol.* **1997**, *6*, 373–385.

(53) Alves, L. L. *Plasma Sources Sci. Technol.* **2007**, *16* (3), 557–569.

(54) Berthelot, A.; Bogaerts, A. *J. Phys. Chem. C* **2017**, *121* (15), 8236–8251.

(55) Berthelot, A.; Bogaerts, A. *Plasma Sources Sci. Technol.* **2017**, *26* (11), 115002.

(56) Pancheshnyi, S.; Eismann, B.; Hagelaar, G. J. M.; Pitchford, L. C. University of Toulouse, LAPLACE, CNRS-UPS-INP: Toulouse 2008.

(57)   Klarenaar, B. L. M.; Engeln, R.; van den Bekerom, D. C. M.; van de Sanden, R.; Morillo-Candas, A. S. S.; Guaitella, O. *Plasma Sources Sci. Technol.* **2017**, *26* (11), 115008.

(58)   Treanor, C. E.; Rich, J. W.; Rehm, R. G. *J. Chem. Phys.* **1968**, *48* (4), 1798–1807.

(59)   Blauer, J. A. *A Survey of Vibrational Relaxation Rate Data Processes Important to CO2-N2-H2O Infrared Plume Radiation*; NTIS, 1973.

(60)   Schwartz, R. N.; Slawsky, Z. I.; Herzfeld, K. F. *J. Chem. Phys.* **1952**, *20* (10), 1591–1599.

(61)   Gamache, R. R.; Lynch, R.; Plateaux, J. J.; Barbe, A. *J. Quant. Spectrosc. Radiat. Transf.* **1997**, *57* (4), 485–496.

(62)   TRINITI database www.lxcat.net/TRINITI.

(63)   Makochekanwa, C.; Kajita, R.; Kato, H.; Kitajima, M.; Cho, H.; Kimura, M.; Tanaka, H. *J. Chem. Phys.* **2005**, *122* (1).

(64)   Yousfi, M.; Benabdessadok, M. D. *J. Appl. Phys.* **1996**, *80* (12), 6619–6630.

(65)   Ness, K. F.; Robson, R. E.; Brunger, M. J.; White, R. D. *J. Chem. Phys.* **2012**, *136* (2).

(66)   Muñoz, A.; Blanco, F.; Garcia, G.; Thorn, P. A.; Brunger, M. J.; Sullivan, J. P.; Buckman, S. J. *Int. J. Mass Spectrom.* **2008**, *277* (1–3), 175–179.

(67)   Ness, K. F.; Robson, R. E. *Phys. Rev. A* **1988**, *38* (3), 1446–1456.

(68)   Satoru Kawaguchi; Takahashi, K.; Satoh, K.; Itoh, H. *Jpn. J. Appl. Phys.* **2016**, *55*, 07LD03.

(69)   Gianturco, F. A.; Thompson, D. G. *J. Phys. B. Atom. Molec. Phys.* **1980**, *13*, 613–625.

(70)   Faure, A.; Gorfinkiel, J. D.; Tennyson, J. *Mon. Not. R. Astron. Soc.* **2004**, *333*, 323–333.

(71)   Jung, K.; Antoni, T.; Muller, R.; Kochem, K.; Ehrhardt, H. *J. Phys. B At. Mol.phys* **1982**, *15*, 3535–3555.

(72)   MacHado, L. E.; Brescansin, L. M.; Iga, I.; Lee, M. T. *Eur. Phys. J. D* **2005**, *33* (2), 193–199.

(73)   Cho, H.; Park, Y. S.; Tanaka, H.; Buckman, S. J. *J. Phys. B At. Mol. Opt. Phys.* **2004**, *37* (3), 625–634.

(74)   Itikawa, Y. *Journal of the Physical Society of Japan*. 1972, pp 217–226.

(75)   Seng, G.; Lindler, F. *J. Phys. B. Atom. Molec. Phys.* **1976**, *9* (14).

(76)   Joshipura, K. N.; Pandya, S. H.; Mason, N. J. *Eur. Phys. J. D* **2017**, *71* (4), 1–7.

(77)   Hayashi, M.; Pitchford, L. C.; McKoy, B. V.; Chutjian, A.; Trajmar, S. *Swarm Studies and Inelastic Electron-Molecule Collisions*; Springer-Verslag: New York, 1987.

(78)   Hayashi database www.lxcat.net/Hayashi.

(79)   Chen, G.; Britun, N.; Godfroid, T.; Georgieva, V.; Snyders, R. *J. Phys. D. Appl. Phys.* **2016**, *50*.

(80)   Berthelot, A. Modeling of microwave plasmas for carbon dioxide conversion, University Of Antwerp, 2018.

Summary

A vibrational kinetics study was performed for a CO_2/H_2O-mixture, to obtain deeper insight in the influence of H_2O on the CO_2 vibrational levels, and more specifically on the asymmetric mode levels. For this purpose, an electron impact cross section set was created for H_2O. Based on this set, the EEDF was calculated for different mixing ratios, showing mostly changes in the < 1 eV region, due to the rotational excitation of H_2O, resulting in the slowing down of electrons. In addition, an increase in the dissociation and ionization rate coefficients was obtained upon higher H_2O additions, due to the higher ionization cross sections of water. The cross section set was incorporated into the Kozak and Bogaerts model.[1] To obtain a better understanding of the vibrational kinetics, the V-T reactions were included in the models of Kozak and Bogaerts[1] and Silva et al.[2] In the first model, this resulted in a slight decrease in the vibrational densities for the lower levels, but showed a small increase at the very beginning of the plasma. These results can be explained by a lower gas temperature, higher electron temperature and additional electron impact reactions. However, these hypotheses should be tested further. The second model of Silva et al. only includes lower lying levels, and therefore only information on the effect on the lower lying levels could be obtained. The simulations showed a quenching of the lower asymmetric mode levels, but had no influence on the other vibrational modes. This is the result of the higher rate constants for the asymmetric quenching reactions by H_2O. Since both models have a different set-up, there are too many variables to compare them. In general it can be concluded that water shows a very complex behaviour in different environments and more research is needed. The results of this research are a first step to more extensive research, that also includes V-V-reactions and chemical processes.

Samenvatting

Deze masterthesis bestudeert de invloed van water op de vibrationele niveaus van water door middel van twee kinetische modellen, ontwikkeld door (i) Kozak en Bogaerts[1] en (ii) Silva et al.[2] Hiervoor werd een elektron impact cross sectie set voor water samengesteld. Hieruit werd een EEDF berekend voor verschillende fracties van water. Het belangrijkste resultaat hieruit situeert zich in de regio < 1 eV, waar de rotationele excitatie van water het belangrijkste inelastische elektronimpact proces is dat leidt tot lagere elektron energieën. Uit de cross sectie set konden ook de reactiecoëfficiënten berekend worden voor de dissociatie en ionisatie door elektron impact. Deze waren hoger voor een hogere fractie van water. Voor de ionisatie is dat te wijten aan de hogere cross secties van water voor dit proces. De cross sectie set wordt gebruikt in het model van Kozak en Bogaerts. Om beter inzicht in de vibrationele kinetiek te krijgen, worden er V-T-reacties van water en CO_2 toegevoegd aan beide modellen. Voor het eerste model resulteert dit in een lichtjes lagere populatie van de vibrationele niveaus. Hier valt wel op te merken dat in het begin van het plasma een toename in populatie optreedt in de hoger gelegen niveaus. De resultaten in het algemeen kunnen verklaard worden door een hogere elektron temperatuur, een lagere gastemperatuur en de extra elektron impact reacties. Door tijdsgebrek konden deze hypotheses echter niet getest worden. In het tweede model van Silva et al, dat zich meer op de lager gelegen niveaus concentreert, werd quenching van de asymmetrische niveaus aangetoond. Voor de symmetrische en bending niveaus was geen verschil zichtbaar. De quenching is het gevolg van de hogere reactiecoëfficiënten die H_2O bevat voor quenching van CO_2. In het algemeen kan geconcludeerd worden dat water quenching vertoont, maar dat er meer onderzoek nodig is naar de onderliggende mechanismen.

Wetenschap Populariserende Samenvatting

De 21ste eeuw wordt getekend door een grote bedreiging: klimaatverandering. Als grote boosdoener wordt er vaak gewezen naar koolstofdioxide of CO_2. Deze molecule heeft de opmerkelijke eigenschap dat het de hitte vasthoudt in de atmosfeer. Vaak wordt vergeten dat nog een andere molecule, namelijk water of H_2O, diezelfde eigenschap bezit. Ze worden daarom broeikasgassen genoemd. In een tijd waar fossiele brandstoffen tot het verleden beginnen te behoren, is er een technologie ontwikkeld die gebruikt maakt van net deze twee interessante moleculen en deze omzet in nuttige producten en brandstof, precies alsof je de tijd terugdraait. Dit is allemaal mogelijk door plasma's. Dit zijn geïoniseerde gassen, die ook terug te vinden zijn in o.a. neonlampen. Indien men CO_2-gas opneemt uit de atmosfeer of de uitlaat van chemische processen, is het in principe mogelijk om deze om te zetten tot methanol, een niet drinkbare alcohol. Niet bruikbaar voor ons, maar een heel belangrijk basisproduct voor de industrie. De atmosfeer echter bestaat uit meer dan alleen CO_2, zoals water, en het is daarom interessant om combinaties te onderzoeken. Dit kan tegenwoordig d.m.v. computersimulaties, waarbij speciale modellen worden ontwikkeld waarbij gespeeld kan worden met verschillende parameters, en deze zo te optimaliseren, om te bouwen aan een nieuwe groenere wereld.

Appendix

CHAPTER 2: Theory and Methods

A1: Constants for calculation of the energies of the vibrational CO_2-levels

Constant	Value (cm^{-1})
ω_1	1354.31
ω_2	672.85
ω_3	2396.32
x_{11}	-2.93
x_{12}	-4.61
x_{13}	-19.82
x_{22}	1.35
x_{23}	-12.31
x_{33}	-12.47
$x_{l_2 l_2}$	-0.97

A2: Vibrational Levels of CO_2

CO_2(State)	Energy (eV)
CO_2(000)	0.00
CO_2(010)	0.08
CO_2(020,100)	0.17
CO_2(030,110)	0.25
CO_2(040,120,200)	0.33
CO_2(001)	0.29
CO_2(002)	0.58
CO_2(003)	0.86
CO_2(004)	1.14
CO_2(005)	1.43
CO_2(006)	1.70
CO_2(007)	1.97
CO_2(008)	2.24
CO_2(009)	2.51
CO_2(010)	2.77
CO_2(011)	3.03

CO$_2$(012)	3.29
CO$_2$(013)	3.55
CO$_2$(014)	3.80
CO$_2$(015)	4.04
CO$_2$(016)	4.29
CO$_2$(017)	4.53
CO$_2$(018)	4.77
CO$_2$(019)	5.01
CO$_2$(020)	5.24
CO$_2$(021)	5.47

A3: Constants for calculations of the energies of the vibrational levels of water

Constant	Value (cm^{-1})
ω_1	3832.17
ω_2	1648.47
ω_3	3942.35
x_{11}	-42.58
x_{12}	-15.93
x_{13}	-165.82
x_{22}	-16.81
x_{23}	-20.33
x_{33}	-47.57

A4: Vibrational levels of water

H$_2$O(State)	Energy (eV)
H$_2$O(000)	0.00
H$_2$O(010)	0.20
H$_2$O(020)	0.39
H$_2$O(100)	0.45
H$_2$O(001)	0.47
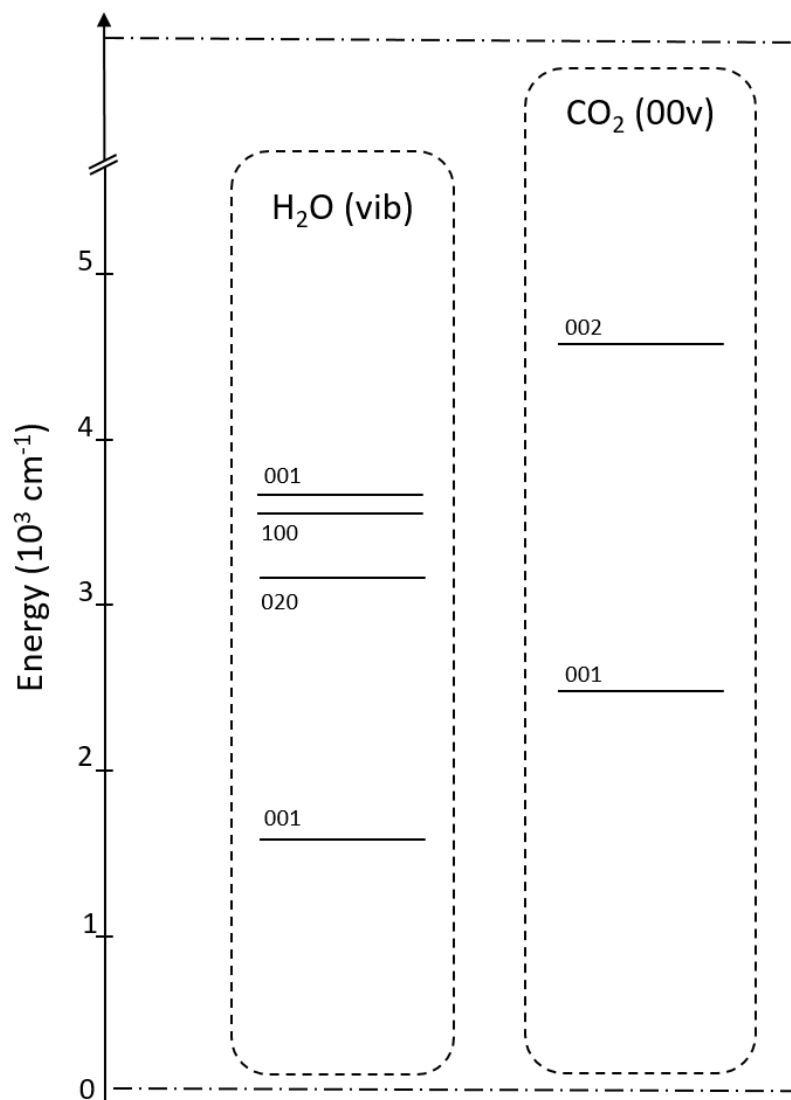
Schematic overview of the vibrational levels of H_2O compared to the asymmetric levels of CO_2.

A5: Fitting constants for the new reactions added to the kinetic CO_2 model

Reaction	Ø	A	B	C
$CO_2(01^10) + H_2O \rightarrow CO_2(00^00) + H_2O$	1.0	31.0	-44.4	242
$CO_2(02^00, 10^00) + H_2O \rightarrow CO_2(01^10) + H_2O$	1.0	29.0	-44.4	242
$CO_2(02^00, 10^00) + H_2O \rightarrow CO_2(00^00) + H_2O$	1.0	26.8	-44.0	242
$CO_2(03^10, 11^10) + H_2O \rightarrow CO_2(02^00, 10^00) + H_2O$	1.0	32.4	-44.4	242
$CO_2(03^10, 11^10) + H_2O \rightarrow CO_2(01^10) + H_2O$	1.0	43.0	-234	525
$CO_2(00^01) + H_2O \rightarrow CO_2(02^00, 10^00) + H_2O$	1.0	27.9	18.5	-211
$CO_2(00^01) + H2O \rightarrow CO2(03^10, 11^10) + H_2O$	1.0	19.3	108	-397
$CO_2(00^01) + H_2O \rightarrow CO_2(01^10) + H_2O$	1.0	30.7	-54.7	-36
$CO_2(04^00, 12^00, 20^00) + H_2O \rightarrow CO_2(00^01) + H_2O$	1.0	29.1	-85.3	159
$CO_2(04^00, 12^00, 20^00) + H_2O \rightarrow CO_2(03^10, 11^10) + H_2O$	1.0	32.8	-44.4	242
$CO_2(0400, 12^00, 20^00) + H_2O \rightarrow CO_2(02^00, 10^00) + H_2O$	1.0	42.2	-215	430

Reaction	Ø	A	B	C
$H_2O(010) + H_2O \rightarrow H_2O(000) + H_2O$	1.0	52.8	-363	1462
$H_2O(020) + H_2O \rightarrow H_2O(010) + H_2O$	1.0	53.5	-363	1462
$H_2O(001) + H_2O \rightarrow H_2O(000) + H_2O$	1.0	55.1	-552	1999
$H_2O(100) + H_2O \rightarrow H_2O(000) + H_2O$	1.0	58.6	-541	2084
$H_2O(001) + H_2O \rightarrow H_2O(100) + H_2O$	1.0	36.9	-88.1	250
$H_2O(010) + CO_2 \rightarrow H_2O(000) + CO_2$	1.0	50.8	-300	813
$H_2O(020) + CO_2 \rightarrow H_2O(010) + CO_2$	1.0	51.5	-300	813
$H_2O(001) + CO_2 \rightarrow H_2O(000) + CO_2$	1.0	55.8	-512	1354
$H_2O(100) + CO_2 \rightarrow H_2O(000) + CO_2$	1.0	57.7	-503	1331
$H_2O(001) + CO_2 \rightarrow H_2O(100) + CO_2$	1.7	36.9	-88.7	250

CHAPTER 3: Results and Discussion

A6 A summary for further reference of this overview is presented below.

This can be used as an easy go to table for further optimization of the set.

Cross Section	Author
Complete Set	Itikawa et al.[43], Ness et al.[65], Munoz et al.[66], Kawaguchi et al.[68]
Momentum Transfer	Gianturco et al.[69]
Rotational	Faure et al.[70], Jung et al.[71], Cho et al.[73], Machado et al.[72]
	Yousfi et al,[64] Itikawa et al.[43,74]
Vibrational	Seng et al.,[75] Makochenkanwa et al.[63]

A7: Cross Sections for CO_2, adopted from the IST-Lisbon set[46] within the LXCat database.
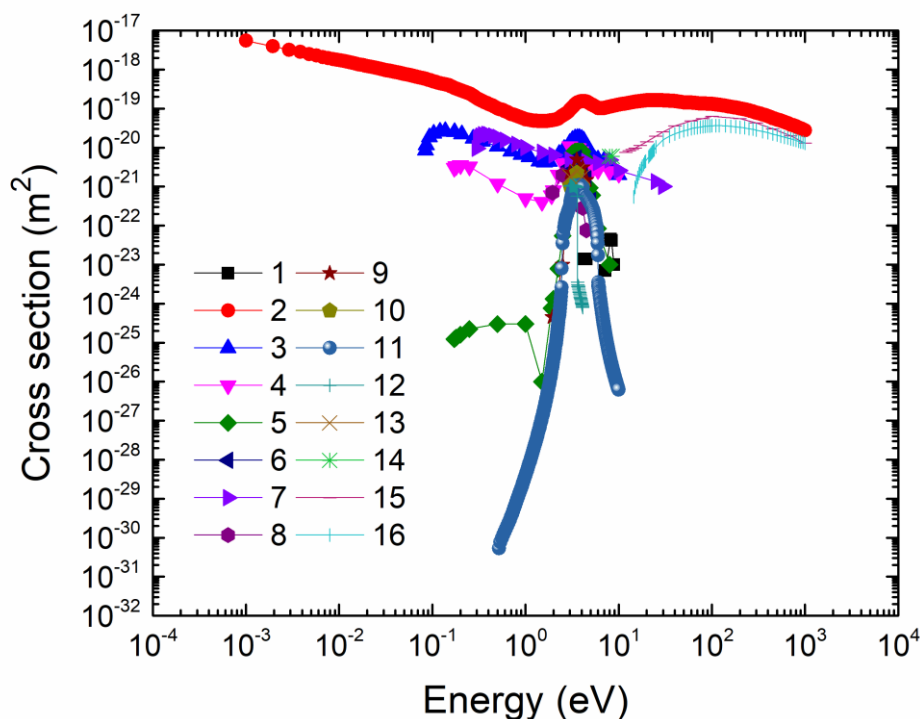
Reaction		Number
Dissociative Attachment	$e + CO_2 \rightarrow CO(X) + O^-(X)$	1
Effective	$e + CO_2 \rightarrow e + CO_2^-$	2
Excitation	$e + CO_2 \leftrightarrow e + CO_2(v=010)$	3
Excitation	$e + CO_2 \rightarrow e + CO_2(v=020)$	4
Excitation	$e + CO_2 \rightarrow e + CO_2(v=100)$	5

74

Excitation	$e + CO_2 \rightarrow e + CO_2(v=030+110)$	6
Excitation	$e + CO_2 \rightarrow e + CO_2(v=001)$	7
Excitation	$e + CO_2 \rightarrow e + CO_2(v=040+120+011)$	8
Excitation 9	$e + CO_2 \rightarrow e + CO_2(X,v=200)$	9
Excitation 10	$e + CO_2 \rightarrow e + CO_2(X,v=050+210+130+021+101)$	10
Excitation 11	$e + CO_2 \rightarrow e + CO_2(X,v=300)$	11
Excitation 12	$e + CO_2 \rightarrow e + CO_2(X,v=060+220+140)$	12
Excitation 13	$e + CO_2 \rightarrow e + CO_2(X,v=0n0+n00)$	13
Excitation 14	$e + CO_2 \rightarrow e + CO_2(e1)$	14
Excitation 15	$e + CO_2 \rightarrow e + CO_2(e2)$	15
Ionization 16	$e + CO_2 \rightarrow e + e + CO_2^+(X)$	16

A8 Ionization Rate coefficients for Water
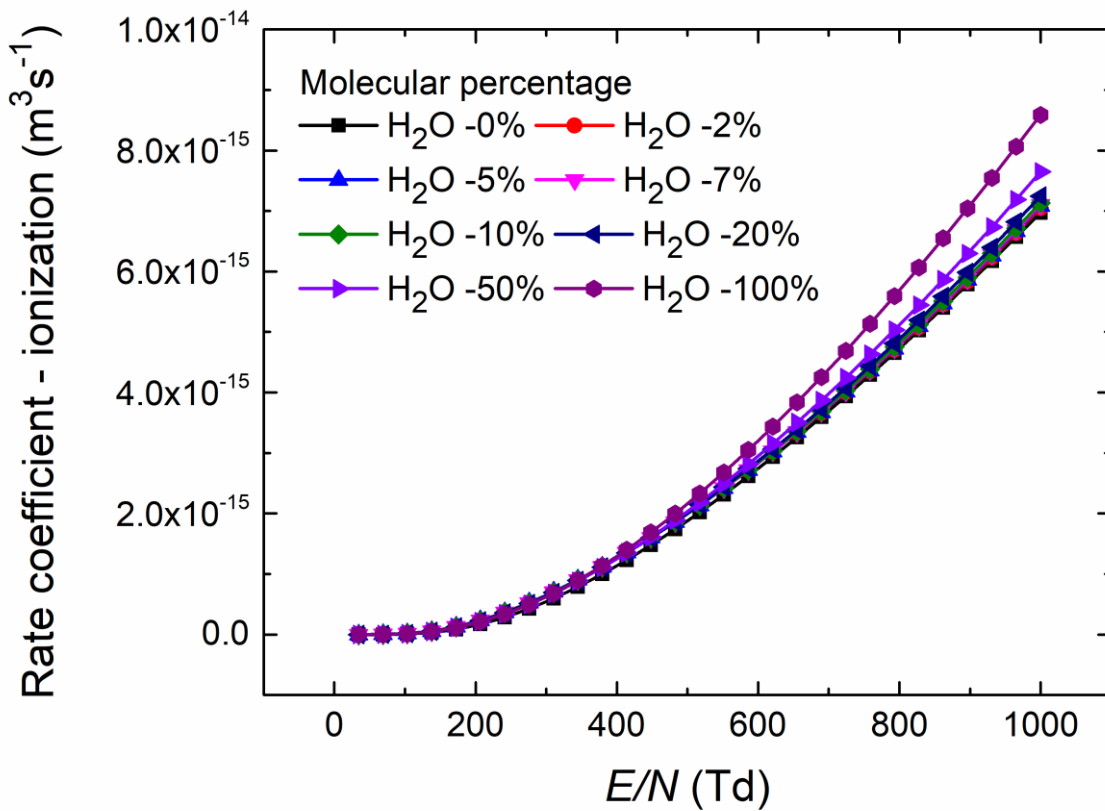
A9: Results from the Kozak and Bogaerts model

In these graphs for each concentration, the vibrational densities for a given position are plotted

(a) 0% of water
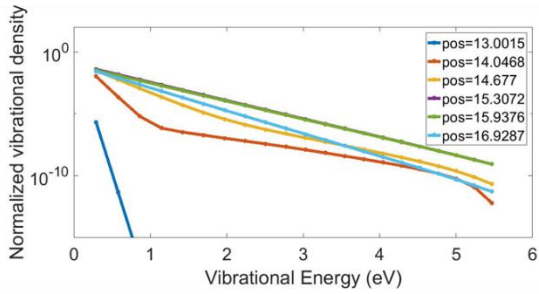
(b) 1% of water
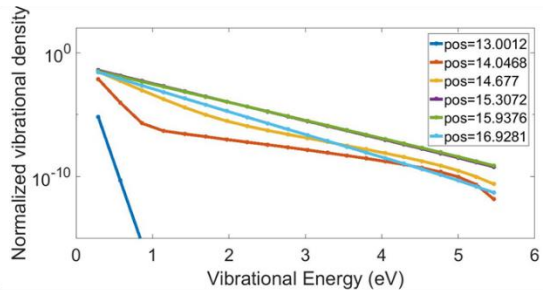
(c) 2% of water
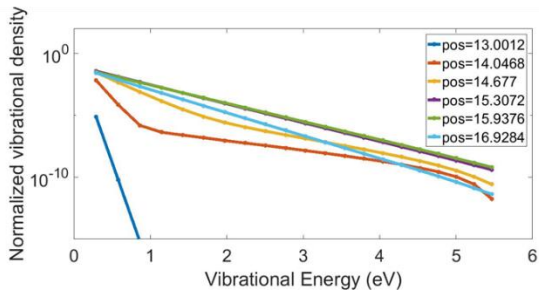
(d) 10% of water
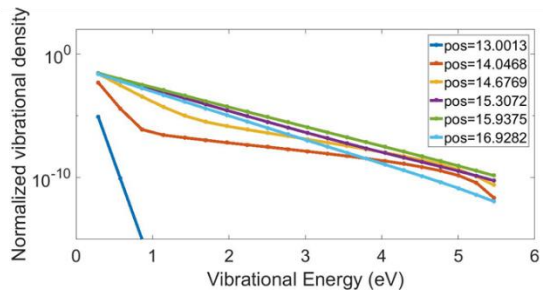
A10: Results from the Silva et al. model

Vibrational densities and temperature for concentrations up to 5% of water.